QUANITFYING SNOW DEPTH

DISTRIBUTIONS AND SPATIAL VARIABILITY

IN COMPLEX MOUNTAIN TERRAIN

by

Zachary Stephen Miller

A thesis submitted in partial fulfillment
of the requirements for the degree

of

Master of Science

in

Earth Sciences

MONTANA STATE UNIVERSITY
Bozeman, Montana

April 2021

ACKNOWLEDGEMENTS

This project would not have been possible without considerable support, time, and effort of many individuals that I am fortunate to be surrounded by. First and foremost, I would like to thank my wife, Grete, and our happy little dog, Blue, who endured countless long evenings, sacrificed time together, and supported me daily throughout the process of completing my thesis project. I would also like to thank my advisor, Dr. Eric Sproles, whose sage guidance helped ensure the entire research process was as smooth as possible. I would also like to thank Dr. Erich Peitzsch, who ensured that my research was robust at each step along the way. Furthermore, I'd like to thank my other committee members, Dr. Karl Birkeland and Dr. Jeffery Deems, for their critical thought and focus.

I would also like to thank Ross Palomaki, Dr. Jordy Hendrix, Zachary Keskinen, Andrew Mullen, and Gabrielle Antonioli for their brainstorming both in the field and around Traphagen Hall. Additionally, I'd like to thank Madeline Beck, Everett Coba, Jon Hageness, Meaghan Gaffney, Ian Hoyer, and Sam Wilson, as well as Bridger Bowl Ski Patrol (Pete Maleski & Bob Petit) and the USFS Custer Gallatin National Forest (Katheryn Barker) who made my extensive field campaign possible and permitted my research on their properties.

I am grateful for the financial support I received from the USGS Climate Change in Mountain Ecosystems group, MSU's Earth Sciences Department, GEOSWIRL research group, and the Montana Association of Geographic Information Professionals. Finally, I am deeply appreciative of all of my family and friends who provided essential encouragement and laughter throughout the entire process.

TABLE OF CONTENTS

TABLE OF CONTENTS CONTINUED

LIST OF TABLES

LIST OF FIGURES

Figure Page

ABSTRACT

The spatial variability of snow depth is a major source of uncertainty in avalanche and hydrologic forecasting. Identification of spatial and temporal patterns in snow depth is further complicated by the interactions of complex mountain topography and localized micro-meteorology. Recent studies have dramatically improved our understanding of snow depth spatial variability by utilizing increasingly accessible remote sensing technologies such as satellite imagery, terrestrial laser scanning, airborne laser scanning and uninhabited aerial systems (UAS) to map spatially continuous snow depths over a variety of spatiotemporal scales. However, much of this work focuses on relatively low-relief topographies or limited temporal frequencies. Our research presents a thorough evaluation of the evolution of snow depth spatial variability at the slope scale in steep complex mountain terrain (45.834 N, -110.935 E) using analysis from UAS imagery.

We apply 13 spatially complete UAS-derived snow depth datasets collected throughout the course of the 2019/2020 winter to analyze spatial and temporal patterns of snow depth and snow depth change variability. Our results show greater spatial variability in steep complex mountain terrain than an adjacent mountain meadow both in the seasonal context and during individual meteorological periods. We analyze 2 cm horizontal resolution snow depth models by (i) comparing spatial patterns with coincident meteorological data, (ii) analysis of the temporal elevation specific patterns of snow depth, and (iii) a comprehensive multi-scalar evaluation of spatial variability. We quantify the unique spatial signature of four specific events: a major snow accumulation, a natural avalanche, a calm period, and a significant wind event. We find a non-linear relationship between elevation and snow depth, with upper elevations proving to be the most variable. We also verify that significant storm events result in the largest snow depth change variability throughout our study area, as compared to other meteorological events.

The synthesis of these findings illustrate the dynamic spatial and temporal snow depth distribution patterns observed in complex mountain terrain during the course of a winter season. These findings are relevant to avalanche forecasters and researchers, snow hydrologists and local water resource managers, and downstream communities dependent on snow as a hydrologic reservoir.

CHAPTER ONE

LITERATURE REVIEW OF SCALE IN THE SPATIAL AND TEMPORAL VARIABILIY OF MOUNTAIN SNOWPACKS

Introduction

Seasonal snowfall is both a natural hazard and natural resource for local mountain and downstream communities worldwide. Snow avalanches have the potential to impact transportation corridors, damage and destroy buildings and infrastructure, and injure or kill humans and wildlife. The snowpack also acts as an essential water reservoir, delaying the release of water frozen in the mountains until later in the water year when the resource is more needed. However, snowpack properties are highly variable over space and time and naturally occur at a variety of scales, making them difficult to research (Schweizer et al., 2008). Scale is paramount to understanding temporal and spatial variability of snow (Blöschl, 1999). Therefore, researching any single piece of the mountain snowpack system must start with a clear acknowledgement of the multitude of spatial and temporal scales constantly at play. In this literature review I use Blöschl & Sivapalan's (1995) scale framework to discuss spatial and temporal variability in mountain snowpacks. By deconstructing complex systems into Blöschl & Sivapalan's three distinct foci - the 'process' scale, the 'observation' scale, and the 'model' scale – I will explore mountain meteorology, snow avalanches, snow modelling, the handling of uncertainty and error, and the scaling relationships that connect these topics.

The Process Scale

The physical properties of snow naturally exist in a wide range of scales. This process scale is defined as "the scale that natural phenomena exhibit and is beyond our control" (Blöschl & Sivapalan, 1995). Spatially, the range begins at the molecular level and quickly grows to approximately 1mm with a condensation nuclei at the onset of growth of a snowflake (McClung & Schaerer, 2006). The spatial process scale of snow properties continues to expand through multiple orders of magnitude to include the continental scale, encompassing >104km^2 interactions of topography and synoptic scale meteorology (Mock & Birkeland, 2000).

"Avalanches are the result of numerous interactions of various contributing factors and processes that act over a large range of different spatial and temporal scales" and, therefore, provide for an excellent example of process scales (Hägeli & McClung, 2004). Large scale circulations, such as the Pacific Decadal Oscillation and the El Ñino/La Ñina Oscillations, influence precipitation patterns and avalanche climates (Mock & Birkeland, 2000). These shifts are especially pronounced in the transitional avalanche climates, where increasing moisture and temperatures can produce more maritime snowpack character and, alternatively, drier and cooler seasons trend towards exhibiting a continental snowpack character. Meso-scale winter weather systems effect individual mountain ranges (10 – 1000 km^2) uniquely and influence regional avalanche formation through spatially variable distributions of precipitation, wind, temperature, and radiation (Birkeland, 2001). Slope scale (0.1 – 10 km^2) interactions with weather determine local avalanche instability, snowpack stratigraphy, avalanche history, local topography and snow depositional patterns (Schweizer & Kronholm, 2007). The micro-scale avalanche processes (<1 m^2), though small, are incredibly relevant as they determine snow grain metamorphism, weak layer continuity, slab and weak layer interface characteristics, sheer and tensile strength, and layer thicknesses (McClung & Schaerer, 2006). As shown in this brief spatial decomposition of avalanche processes, the constant interactions of the individual snowpack processes make defining the spatial process scale of a given property challenging to pin down. Further complexity is added to identifying appropriate process scales when viewed through a temporal lens.

"Due to snow internal processes – following from the fact that snow exists close to its melting point – the spatial variability of the snowpack is expected to change over time" (Schweizer et al., 2008). A snowpack's physical processes exist from fractions of a second, as with fracture initiation during avalanche release, to seasonal and even decadal scales, where snow evolves into firn and global climatic oscillations influence snow accumulation (McClung & Schaerer, 2006). The classic example of the variety of temporal process scales follows a snowflake through its lifecycle as a snow grain. Once a snowflake has formed in the atmosphere, it will continuously evolve until it eventually melts or sublimates into a different physical state. Similarly, the surface of the snowpack interacts with meteorological phenomena along different timelines that include the processes of growing surface hoar, crust development, diurnal recrystallization, wind redistribution, sastrugi growth, slab compaction, and sluffing. Below the surface, the snowpack evolves and the metamorphic processes of faceting, rounding, and sintering all happen along similar but unique temporal scales (McClung & Schaerer, 2006). The movement of water in and through the snowpack also follows its own unique seasonal timeline and that evolution from dry through the pendular and funicular phases is different each year (Gillan et al., 2010). These processes can exist simultaneously in a matter of seconds and over the course of months. This cumulative temporal process scale is often how we begin to comprehend snow stability, with the idea that all snow stability estimates begin with the first snowfall of the season (LaChapelle, 1980).

As McClung & Schaerer (2006) assert, the temporal and spatial variability of a constantly evolving snow stability represent two main challenges of avalanche forecasting. Searching for and identifying overlapping patterns in spatial and temporal process scales are key to delving into researching these physical processes. Despite the challenge of multitude of natural process scales simultaneously occurring and a recognition that observing and modeling a single scale is insufficient for complete understanding of a process, researchers must choose and clarify the most appropriate scale for accurately addressing their research questions. To quote Blöschl (1999), "…the true spatial variability, i.e. the true snow hydrological process which, however, will never be known in full detail."

The Observation Scale

The observation or 'measurement' scale is defined by Blöschl & Sivapalan (1995) as the spatial or temporal 'extent' of a data set, the 'spacing' or time between samples, and the integration volume or 'support' of a single sample. 'Extent', 'spacing', and 'support' are known as the scale triplet and form the foundation of all discussions of the observation scale. The range with which each of these varies depending on the instrument or sensor used to collect data. A precise understanding of the scale triplet for a given observational tool is required for robust data collection when oriented at a measuring a specific process and aligning as closely as possible with its natural scale. Different measurement scales can result in the finding of different spatial or temporal patterns that may, or may not, represent the true process scale (Schweizer et al., 2008). Recognizing these scaling differences is not always obvious when utilizing multiple sensors to observe a specific phenomenon. Hanzer et al. (2016) presents a comprehensive table and compelling graphics to describe the spatial and temporal scale triplets of the validation data sets used in their modelling of SWE. Though this clarity is not always the norm in the literature, identification of the differences between the observation scales of multiple methods and their differences with the true process scale is essential in understanding uncertainty and quantifying error in measurements. The inherent differences between the true process scale and the observations resultant scale are the core of what Blöschl &

Sivapalan (1995) describe as 'scaling issues'; referring more broadly to any difficulties faced when attempting to align measured and modelled scales with process scales.

Uncertainty arises with these 'scaling issues' and must also be understood as an essential component of the observation scale. LaChappelle (1980), then later McClung & Schaerer (2006), describe a three-tiered system of gradually less entropic data used in the practice of avalanche forecasting. The highest level (high entropy) includes meteorology data which is followed by snowpack structure (medium entropy) and snow mechanics (low entropy). This theoretical space reflects the levels of uncertainty accompanying each tool the forecaster has at their disposal and parallels the reality of researchers selecting appropriate sensors for measuring natural processes. Additionally, increasing the scale of focus for an avalanche forecast or a research question inherently introduces greater uncertainty due to the increasing interactions of outside processes and our ability to assess their influence (Schweizer & Kronholm, 2007). The final distinct idea discussed in scaling issues with regards to the observation scale is that of sampling error. Smyth et al. (2020) discusses the importance of understanding the precision of an instrument because its errors will propagate through any further analysis and modelling. Their findings demonstrated that sensor sampling error had a larger influence than observation timing effects on the modelled SWE error and uncertainty. As described, 'scaling issues' largely exist due to a difference in the measured scale from the true process scale.

There are many methods for addressing and minimizing scaling issues in the observation scale. Repetitive measurement, overlapping scales, and cross-validation with different instruments are all central features of these approaches. Lutz & Birkeland

(2011) present a streamlined method by clearly identifying the scale at which their problem lies (surface hoar distribution at the slope scale) and focused their measurements on a variety of processes that encompassed and overlapped that scale. Goetz & Brenning (2019) discuss the utility of completing thorough uncertainty analysis at each independent step as a method for having accurate understanding of potential error in their eventual models. Multiple sources emphasize the necessity of verification of remotely sensed data with near-surface measurements (Avanzi et al., 2017; Bühler et al., 2016; Currier et al., 2019; Dozier et al., 2016; Kinar & Pomeroy, 2015; Marti et al., 2016; Saloranta, 2016; Smyth et al., 2020). Central to understanding the observation scale, the scale triplet, and scaling issues within measurements is having a thorough understanding of the tool being used to answer questions about a specific process scale.

The Model Scale

The model scale is not as clearly defined in the literature, but is established as the modelled extent, spacing, and support of a process. Applying the scale triplet to an output model is essential for both the understanding of a model's scaling interactions with the observations driving it and the true process scale it attempts to replicate. The model scale is unique in that the researchers decide which resolution they are aiming to achieve to replicate and explore the natural process in question. Given that numerical models are either run on or calibrated by observations, measurement scale errors and uncertainty continue to propagate through to the results unless they are explicitly addressed (Avanzi et al., 2017). A distinct shift in constraining modelling error and minimizing scaling issues has been through the increased use of data assimilation as described thoroughly in the snow hydrology literature (Avanzi et al., 2017; Dozier, 2011; Dozier et al., 2016; Saloranta, 2016; Smyth et al., 2020). Similarly, the recent evolution of remote sensing tools relevant to snow spatial and temporal variability research, and especially that of UAS-captured data, require thorough accuracy assessments (Bühler et al., 2016; Currier et al., 2019; Goetz & Brenning, 2019; Harder et al., 2016; Marti et al., 2016).

One scaling issue that is unique to the model scale is that of up- and down-scaling data (Blöschl & Sivapalan, 1995). This is an incredibly relevant 'scaling issue' as re-scaling of modelled data is necessary in nearly all cases because of the differences inherent between the true process scale, the data observed in the measurement scale, and the resultant modelled output scale. The spatial and temporal variability of snowpack properties, in combination with complex mountain terrain interactions, make scaling a challenging and ever-present problem. A key component in addressing this issue is finding and using shared variables across multiple scales (Birkeland, 2001; Schweizer et al., 2008; Smyth et al., 2020). By focusing on a snowpack property that spans multiple spatial or temporal scales, patterns can be used to interpret results and re-scale data appropriately while retaining its natural variability.

A final step in ensuring that the model scale is accurately resolved is through model validation. Hägeli & McClung (2004) discuss the necessity of utilizing information from each scale interacting with the system in appropriate modelling of avalanche prediction. Hanzer et al. (2016) thoroughly addressed possible scaling issues by explicitly listing the scale triplet for each of the validation data sets used and demonstrating their complete coverage of the temporal and spatial scales in question. His method establishes the utility of using multiple overlapping data sources to assess the accuracy of the single source under question. Currier et al. (2019) also identified a significant lapse in validation methods for airborne lidar sensing of snow depth and provided a robust validation technique by focusing on matching spatial resolutions rather than simply relying on point measurement verification. A final novel method for validation was discussed by Goetz & Brenning (2019) that used repeated thorough error analysis of UAS acquired data to arrive at a more holistic uncertainty understanding of their model. Error and uncertainty are inextricably tied to the modelling of different snow processes and acknowledging and addressing those problems through the lens of the scale triplet is critical.

Conclusions on Scaling

The spatial and temporal variability of snowpack properties is widely accepted yet has suffered from a lack of comparability of studies due to the inconsistent usage of the scale triplet (Schweizer et al., 2008). Applying Blöschl & Sivapalan's (1995) scale framework is essential in observing, analyzing, and interpreting spatial and temporal variability in mountain snowpack systems. Researchers utilize overlapping variables as proven through quantitative methods and statistics to understand spatial variability similar to the way avalanche forecasters use repetitive and iterative qualitative observations to assess hazard. Correlation is key in identifying patterns in spatial and temporal variability that we use to understand snowpack processes. Whether used for regional avalanche forecasting, slope-scale snow depth variability mapping, or continental scale snow-water-equivalent estimates, an inductive interpretation of multiple scales and sources of data must be used to formulate a single cohesive answer to the question proposed. As demonstrated in the findings of this literature review, scale should form the foundation of any exploration of snowpack properties and an acknowledgement of the multitude of scales constantly interacting in the system must be addressed.

CHAPTER TWO

SNOW DEPTH DISTRIBUTIONS AND SPATIAL VARIABILITY IN COMPLEX MOUNTAIN TERRAIN

1. Introduction

Seasonal mountain snowfall is a natural resource and natural hazard for nearby and downstream communities. Understanding the evolution of seasonal snow depth, defined as the vertical distance from the snow surface to the base of the snowpack (Fierz et al., 2009), is critical for avalanche forecasters, water resource managers, and local governments. However, quantifying snow depth across the landscape is challenging due to its high spatial variability, especially in mountainous terrain, and the multi-scalar nature of its natural processes (Bühler et al, 2016; Egli et al, 2011; Elder et al., 1998; Grünwald et al., 2010; Schweizer et. al, 2008). Prior studies demonstrate the value of the slope scale for exploring the complex nature of snow depth variability (Anderton et al., 2004; Deems et al., 2013; Eberhard et al., 2021, López-Moreno et al.; 2015, Wirz et al., 2011). In this study, we explore the evolution of spatial snow depth patterns at high resolution on the slope scale over the course of an entire winter season.

The slope scale, here defined as < 0.2 km^2, is an optimal spatial extent for examining snow depth variability and is essential for understanding avalanche formation processes. Schweizer et al. (2008) emphasize that the variable nature of snow cover is the primary factor in uncertainty for avalanche and slope stability predictions. Much of the avalanche spatial variability research focuses on the spatial distribution and interactions of different layers within the snowpack and their effects on stability (Conway and Abrahamson, 1986; Jamieson and Johnston, 1992; Birkeland et al., 1998; Landry 2004; Kronholm and Schweizer, 2003; Birkeland et al., 2004; Logan et al., 2007; Lutz et al., 2007; Hendrix et al., 2009; Lutz and Birkeland et al., 2011; Reuter et al., 2016). Snow stability is similar and inherently tied to snow depth in that both are spatially and temporally variable across a variety of scales. The interactions of snow depth and snowpack stability are essential in snow avalanche processes at the slope scale (Birkeland et al., 1995).

The spatial variability of snow depth in complex mountain terrain has yet to be thoroughly addressed and requires centimeter-scale spatial resolutions due to micrometeorological effects on snow accumulation, ablation, and re-distribution. These centimeter-scale distribution patterns have direct effects on avalanche formation and, as a result, an avalanche's ability to rapidly change the spatial distributions of snow depth in mountain terrain (Kronholm and Birkeland, 2005; McClung and Schaerer, 2006; Logan et al. 2007; Schweizer et al., 2008; Lutz and Birkeland, 2011; Schweizer et al., 2016). Unique centimeter-scale processes and patterns in complex terrain evolve throughout the course of an entire winter and differ when compared to more homogenous simple terrain. The snowpacks of different terrains are influenced by the local interactions of weather and slope scale topography. In this study, we define complex terrain as steep mountainous topographies including hillslopes > 25° with interspersed rock outcrops, vertical cliff features, and variable slope geometries.

A major challenge in accurately analyzing the spatial variability of snow depth is acquiring measurements at an appropriate spatial resolution (Clark et al., 2011; Kinar and Pomeroy, 2015; Meyer and Skiles, 2019). Traditional methods of measuring snow depth include snow surveys, where point measurements are collected through manual probing of the snow along established survey routes, and automated weather stations (AWS), where a sensor records snow depth measurements at a single location over a period ranging from hours to years (Kinar and Pomeroy, 2015). These snow depth measurements are often combined with snow density measurements to gather snow water equivalent (SWE) information for quantifying water stored in the snowpack. While these methods are still used as proxies for watershed-scale snow depth and water storage estimations, they provide a spatially incomplete picture of snow depth and SWE distributions due to their limited measurement areas (Elder et al., 1998; Dozier, 2011; Dozier et al., 2016). This is problematic because snow depth distributions are not uniform across the landscape, and single point measurements do not adequately represent this spatial variability. Point measurement collection is also limited by avoiding exposure to snow avalanches and therefore measurements collected from relatively flat, planar terrain are overrepresented compared to measurements from steeper slopes. One method to overcome sparse spatiotemporal measurements are model-based simulations of the snowpack. Physical snowpack modeling, such as SNOWPACK (Lehning et al., 1999) and SnowModel (Liston and Elder, 2006), integrate meteorological inputs to simulate a snowpack at a single location or a grid of locations and have improved to the point of resolving down to grid sizes of 1 m^2 across various topographies (Sproles et al., 2013).

These methods show tremendous promise, yet are limited by the quality of their validation and input data, and are challenged by the inherent complexities of heterogeneous mountain terrain.

Remotely sensed measurements provide an obvious answer to quantifying snow depth variability in complex terrain, but come with a necessary compromise between spatial resolution and measurement extent. Satellite-acquired snow depth data provide spatially continuous coverage within a single pass's sensor swath, but at insufficient spatial resolutions to observe slope-scale variability and insufficient temporal resolutions to capture the effects of individual weather events in many mid-latitude locations (Kinar and Pomeroy, 2015; Marti et al., 2016; Sproles et al., 2020). Despite achieving ground sampling distances of 1.24 m/pixel resolution (WorldView-3 and WorldView-4 satellites), the vertical accuracy of surfaces acquired through these satellite multiband images and photogrammetry is still insufficient (0.62 m) to resolve for the centimeter scale snow depth changes essential for assessing avalanche formation processes (Hu et al., 2016). Terrestrial laser scanning provides exceptional accuracy and precision when examining snow depth at the slope scale, but can be limited by field of view terrain obstacles such as rock outcrops (Deems et al., 2013; Wehr and Lohr, 1999; Wirz et al., 2011). Airborne laser scanning circumvents such field of view obstacles, but still remains prohibitively expensive for many watersheds and regions (Bühler et al., 2015; Painter et al., 2016; Meyer and Skiles, 2019; Brandt et al., 2020). Airborne photogrammetry provides comparable snow depth measurements as airborne laser scanning, is effective in complex terrain, but is relatively expensive (Meyer et al., 2021). The recent development of Uninhabited Aerial Systems (UAS) and structure-from-motion (SfM) photogrammetry offer similar precision as laser scanning and airborne photogrammetry at the slope scale, with relatively low cost and minimal terrain or temporal limitations (Bühler et al., 2016; Gaffey and Bhardwaj, 2020; Eberhard et al., 2021).

UAS provide overlapping aerial photography along specific survey flight paths, providing ideal inputs for SfM photogrammetry processing (Watts et al., 2012; Colomina and Molina, 2014). Images are embedded with a geospatial reference, allowing SfM photogrammetric processing to match points (tie points) in overlapping imagery with precise spatial reference data. These points are used for the interpolation of surfaces and terrain in three-dimensional space (Westoby et al., 2012; Nolan et al., 2015; Smith et al., 2016). UAS-derived snow depth models utilize digital surface model (DSM) or point cloud differencing techniques where a reference surface is subtracted from the surface in question to calculate a difference surface (Bösch et al., 2016; Redpath et al., 2018). These differenced surfaces provide a unique insight into snow depth variability and distribution if accurately collected at sufficient spatial resolution (Eberhard et al., 2021). Numerous studies conclude that UAS and SfM techniques are effective at mapping snow depth variability at the slope scale, yet most focus on simpler terrain and only compare two individual timestamps of data (Vander Jagt et al., 2015; Bösch et al., 2016; Bühler et al., 2016; De Michele et al., 2016; Harder et al., 2016; Cimoli et al., 2017; Adams et al., 2018; Avanzi et al., 2018; Redpath et al., 2018; Peitzsch et al., 2018; Gabrlik et al., 2019; McCormack and Vaa, 2019; Eberhard et al., 2021).

Studies of snow depth variability cover a variety of spatial and temporal scales (Blöschl & Sivapalan, 1995; Birkeland et al., 2001; Schweizer et al., 2008; Egli et al., 2011; López-Moreno et al., 2015; Mendoza et al., 2020). Looking specifically at UAS snow depth variability studies, De Michele et al. (2016) found that mapping snow depth variability below the decimeter scale (10 or 20 cm) was unnecessary at peak accumulation over a small alpine catchment (0.3 km^2) because of the homogeneity of snow depth distribution at peak accumulation and recommended a multitemporal approach be utilized in future research. Redpath et al. (2018) concluded that measuring snow depth with decimeter-level accuracy is sufficient for observing seasonal snowpack processes across entire hydrologic catchments (0.41 km^2), including some complex terrain, and that UAS derived measurements of snow depth provide the opportunity to explore spatial variability at scales permitting micro terrain and meteorological effects to be considered.

The objective of this work is to assess the influence of specific meteorological periods on the spatial variability of snow depth at the slope scale. This research is necessary to further our understanding of meteorological effects on snow depth variability, snow depth variability differences in steep complex mountain terrain and relatively simple terrain, and the seasonal evolution of snow depth variability patterns at high resolution over the course of an entire winter. We conducted an extensive winter field campaign in the Bridger Mountains of Montana, USA throughout the 2019-2020 winter (December-May). We collected UAS surveys, sub-weekly traditional manual snow depth measurements, and temporally continuous automated snow depth data. Our research is designed to (1) explore the intersection between snow depth change distribution and meteorological events at the slope scale, (2) analyze evolving spatial and elevational patterns of snow depth variability at the slope scale over the course of an entire winter, and (3) examine the effects of scale size on spatial variability of snow depth and snow depth change.

Therefore, the research questions we address in this paper are:

1. How do individual meteorological periods influence spatial snow depth change patterns at the slope scale?
2. How do snow depth distributions evolve across varying elevations temporally?
3. What spatial resolutions of snow depth measurements are required to effectively represent snow depth variability at the slope scale?

2. Study Locations

We selected two adjacent study sites in the Bridger Mountains of southwest Montana, USA (45.834 N, -110.935 E), the Hourglass Couloir and Brackett Meadow (Figure 1). The Bridger Range is classified as an intermountain snow and avalanche climate, which are characterized by average December through March temperatures > -7°C and annual snowfall > 560 cm (Mock, 1995; Birkeland and Mock, 1996; Mock and Birkeland, 2000). This area, also referred to as Wolverine Basin, has been the site of frequent snow and avalanche research over the past 20 years (Lundy et al., 2001; Deems, 2002; Landry et al., 2004; Van Peursem et al., 2016). We chose these sites because they exhibit distinct mountain topographies but are subject to nearly the same meteorological conditions.

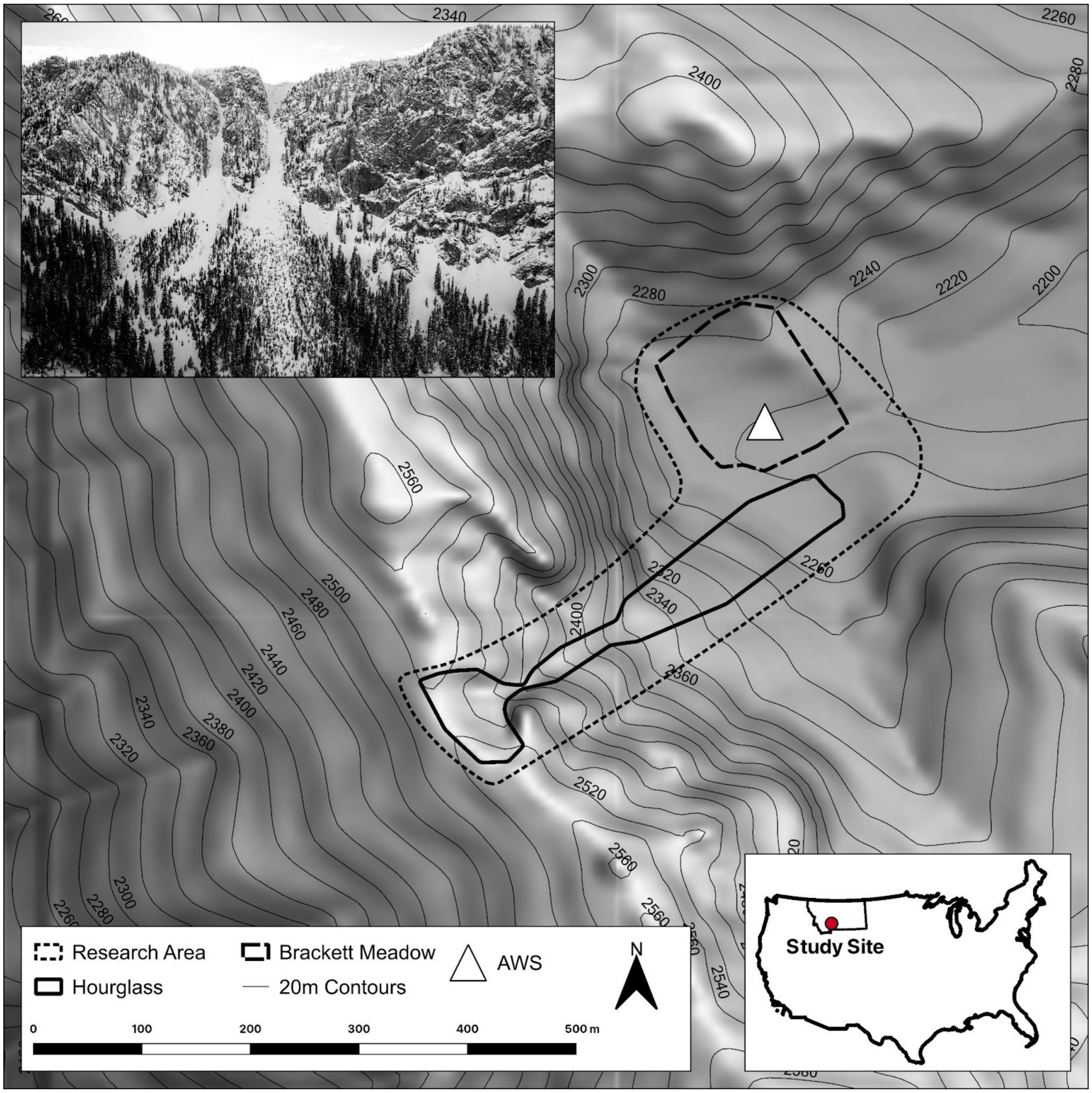

Figure 1: Overview of study location in the Bridger Range of Montana, USA with the research area (dotted polygon), the Hourglass site (solid polygon), Brackett Meadow site (dashed polygon), and the Hourglass AWS (triangle) shown. Photograph of the Hourglass site (center chute) in the upper left. Data map source: U.S. Geological Survey, 2017.

2.1 The Hourglass: steep, complex mountain terrain

The Hourglass couloir site (henceforth called "the Hourglass") is a sub-alpine avalanche path located at an elevation of 2400 m.a.s.l. The slope faces predominately northeast and is 550 m long, 300 m tall with an approximate area of 53000 m^2 (Figure 1).

The mean slope angle of the Hourglass is 33°, and ranges from 5° to 90°. The ground surface of the Hourglass is mainly composed of rock scree, outcrops of limestone cliffs, and 1 - 2 m subalpine fir and engelmann spruce trees in the avalanche path. Mature trees 10 - 20 m tall and 1 m shrubs/bushes border the main avalanche path. Frequent ridgetop wind-loading from dominant westerly storms results in large cornice growth during the winter along the top of the couloir. Nearby Bridger Bowl Ski Area reports an average of 6.5 m of annual snowfall which, when combined with wind, contributes to frequent small avalanches within the avalanche path (Lundy et al., 2001). The snow in the Hourglass is generally undisturbed by humans due to its consequential avalanche potential, yet backcountry skiers frequently cross the flat terrain below. Additionally, the Hourglass sits at the hydrologic top of the South Fork of Brackett Creek, within the Brackett Creek watershed.

2.2 Brackett Meadow: flat, sheltered meadow

The Brackett Meadow site is a mountain meadow located at the headwaters of the South Fork of Brackett Creek in the Bridger Mountains. It sits at an average elevation of 2240 m a.s.l. and is adjacent to the Hourglass site (Figure 1). Brackett Meadow is approximately 35000 m^2 and has a mean slope of 5°. It is covered by a mix of grasses and shrubs with 10 - 20 m mature coniferous forest on its north, west, and south sides. The meadow is 1 and 2 km, respectively, from two AWSs at Bridger Bowl Ski Area: "Alpine" (2286 m) and "Ridge" (2591 m). It is located 4.5 and 6 km, respectively, from two NRCS SNOTEL sites: "Sacajawea #929" (1996 m) and "Brackett Creek #365" (2231 m). For this study, we installed an additional AWS in Brackett Meadow which collected hourly temperature, relative humidity, wind speed, wind direction, net radiation and snow depth measurements from November 6, 2019 to June 10, 2020. The relatively flat forest opening of the Brackett Meadow site is sheltered from all but easterly wind directions and localized severe weather by the surrounding dense forest and steep 300 m headwall to its west. Brackett Meadow's below-treeline, wind-protected location is similar to many SNOTEL sites (Molotoch and Bales, 2005).

3. Methods

Our study aims to quantify the effects of individual weather events on snow depth variability throughout an entire winter season. To observe these influences we collected data before and after storm events to observe centimeter scale changes in snow depth throughout the entire study site. We present data from UAS surveys on 13 field days that captured the effects of 7 storm and 5 non-storm meteorological periods during the 2019-2020 winter. We design our surveys to achieve horizontal spatial resolutions of < 5 cm to optimally observe individual storm snow depth change (De Michele et al., 2016; Fierz et al., 2009). We compare our UAS-based measurements with traditional snow depth measurement techniques and meteorological measurements collected by the AWS throughout the winter. Our data collection was limited by the onset of the COVID-19 pandemic, as a result a large temporal gap in field days exists between March 17 and May 14, 2020.

3.1 UAS Surveys

We used a commercially available DJI Phantom 4 UAS equipped with a 20-megapixel camera and Real-Time-Kinematic (RTK) Global Navigation Satellite System (GNSS). We conducted repeated pre-planned missions flying the UAS autonomously in a grid pattern over both the Hourglass and Brackett Meadow sites, collecting approximately 550 overlapping images per field day. Our mission parameters are similar to those found in Goetz & Brenning (2019), employing 70% front/side image overlap, a gimbal angle set to 20° off nadir to compensate for the steep slope in the Hourglass, 50 m above-ground-level (AGL) flight altitude, yielding an estimated ground sampling distance (GSD) of < 2 cm per pixel. We flew the UAS in a wide variety of lighting and meteorological conditions with temperatures ranging from -15 to 10°C and ridgetop winds gusts up to 9 m/sec (see Appendix B Table 1 for flight details).

To constrain topographic error in post-processing, we collected 25 stationary and easily recognizable ground control points with high-resolution RTK GNSS survey equipment during the snow-free season to incorporate into the models. Due to variable snow cover, we used a partial selection of the 25 ground control points in each individual model. Ground control points ensure models are geolocated in the correct physical locations. We deployed and surveyed validation point (VP) targets prior to flights in safe accessible locations within the study area and measured snow depth at each VP immediately after the flights. VPs are used for error assessment in modeled snow depth measurements.

3.2 Processing Methods

We process the overlapping imagery to derive snow depth change maps using three steps: (1) Post-Processing-Kinematic (PPK) location corrections, (2) SfM processing of imagery for digital surface model (DSM) creation, and (3) DSM-differencing to derive snow depth changes (Figure 2).

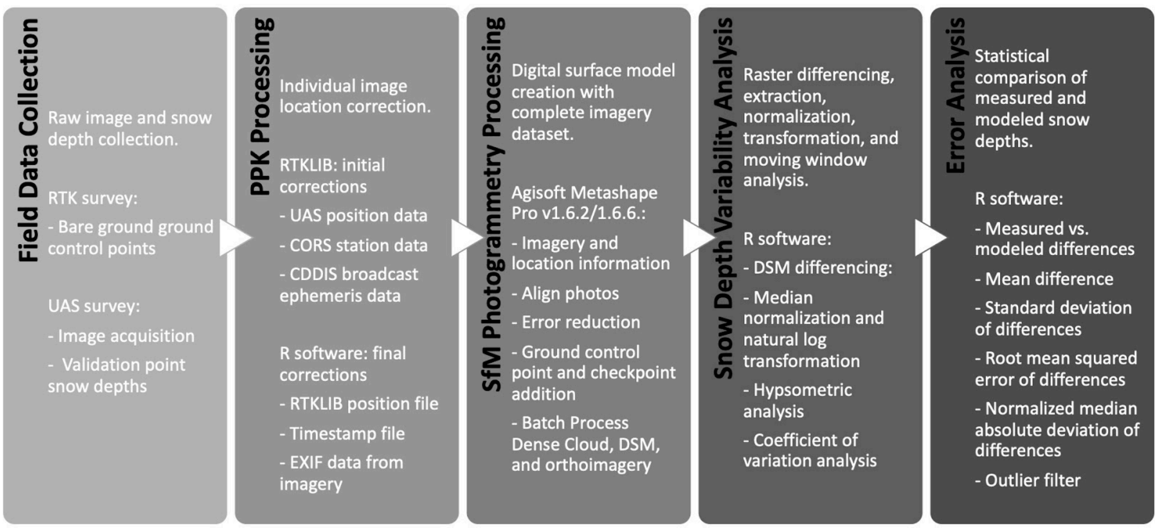

Figure 2: UAS - Structure from Motion photogrammetry workflow. Each panel represents a step in the process of our methods and includes a brief description of the purpose (top comment), the software used (sub-headings), and data or steps included (bulleted list).

We post-process the UAS location data to improve the quality of the RTK GNSS positions and ensure accurate co-registration of output models using RTKLIB (Takasu, 2009) and R software environment (R Core Team, 2019) in the WGS84 geographic coordinate system (EPSG::4326). We use the MTSU reference station (~21 km from the study site), the National Aeronautics and Space Administration's daily Global Positioning Systems broadcast ephemeris data, and the UAS RINEX and Timestamp files. PPK processing results in positional accuracies of < 10 cm for most UAS photo locations.

We completed SfM photogrammetry processing using the software package Agisoft Metashape Pro Version 1.6.2/1.6.6 (Agisoft, 2020), which generates 3-D surface models from overlapping imagery and point matching (Alidoost & Arefi, 2017; Bühler et al., 2016; Carbonneau & Dietrich, 2017; Cimoli et al., 2017; De Michele et al., 2016; Gabrlik et al., 2018, 2019; Nolan et al., 2015). We filtered, aligned, and reduced the error of the geolocated imagery before the addition of GCPs for final batch processing (Table 1). Finally, we ensured accurate co-registration by aligning the vertical and horizontal positions of the models to available snow-free ground control points. This processing workflow produces a dense point cloud, interpolated polygonal mesh model, 3-D model, digital surface model (DSM) and orthomosaic that can then be used for snow depth change analysis.

Estimated Image Quality Threshold	**Photo Alignment - Key Point Limit**	**Photo Alignment - Tie Point Limit**	**Reconstruction Uncertainty**	**Projection Accuracy**	**Reprojection Error**	**Dense Cloud Quality and Depth Filtering**	**Mesh Depth Map Quality and Face Count**	**DEM Quality and Source**
0.7	40,000	10,000	20-25	2.75-3.0	0.3	High, Aggressive	High, High	High, Dense Cloud

Table 1: Agisoft Metashape processing settings. Refer to Appendix A Glossary 1 and Agisoft (2020) for parameter definitions.

3.3 DSM Selection

We filter our DSM datasets by removing field days with resultant DSMs of > 2 cm resolution (n = 8), field days with incomplete DSMs due to cloud cover and low light (n = 4), and field days with uncorrectable instrument error (n = 1) (Table 2). Our filtering results in analysis of 13 (12 snow-on and 1 snow-free) of the original 26 flight days.

Reason for Removal	**Sampling Dates (YYYY-MM-DD)**
Insufficient resolution (> 2 cm resolution)	2019-11-11, 2019-11-14, 2019-11-21, 2019-12-03, 2019-12-10, 2019-12-16, 2019-12-19, 2020-01-03
Incomplete model (clouds and fog)	2020-01-28, 2020-02-10, 2020-02-18, 2020-02-25
Instrument error (positioning malfunction)	2020-01-21

Table 2: DSM removal reasons and sampling days.

3.4 Manual Snow Depth Collection

Throughout the 2019-2020 winter, we collected traditional manual snow depth measurements through probing and snow surveys within the research area as well as pit profiles on adjacent slopes. To determine the 1 m^2 average, variation, and range measurements at VPs, we probed manual in-situ snow depths at the center and four corners of each deployed marker. We measured snow height and SWE using a federal snow sampler (Water Supply Forecasting Unit, 1984) at 10 geolocated and randomly sampled points in the Brackett Meadow during monthly snow surveys. We collected location information for each of these manual snow depth measurements with handheld GPS units (3 - 5 m accuracy). These geolocated VP and snow survey snow depths are used for error assessment of modelled snow depths. We documented weekly full depth pit profiles in accordance with Snow, Weather and Avalanches: Observation Guidelines (Greene et al., 2016), including measures of total snow depth, individual snow layer depth, grain type and size, layer hardness, stability tests, a temperature profile, and snow density collected every 10 cm for each pit. Additionally, we collected a single avalanche crown profile in the Hourglass on February 28, 2020 which included total snow depth, individual snow layer depth, grain type and size, and a stability test. Summary statistics were calculated for manual snow depth measurements and their modelled equivalent depths for each field day (Appendix B Table 2).

3.5 Analysis Methods

We analyze our observations to assess for changes in snow depth variability both spatially and temporally. We begin with an assessment of error between modeled snow depths and manually measured in-situ snow depth measurements. We calculate the differences between measured and modeled snow depth data for each in-situ probed VP and snow-survey measurement. We then calculate mean, standard deviation, root mean square error (RMSE), and normalized median absolute deviation (NMAD) values for the differences between modeled and measured snow depths following a condensed version of the accuracy and precision measures presented in Adams et al. (2018) and Eberhard et al. (2021). The mean difference and RMSE are common measures of accuracy. Standard deviation and NMAD are common measures of precision, with NMAD being more resistant to outliers. To observe the effect of outliers on the accuracy and precision of our modeled snow depths, we filter outlier errors greater than 3 standard deviations (Höhle and Höhle, 2009) and recalculate the mean and standard deviation values.

To explore the meteorological effects on the spatial distributions of accumulation and ablation for individual time steps, we examine snow depth change maps from individual time steps in comparison with in-situ AWS data from three nearby stations. We explore the meteorological influences of snow accumulation, a natural avalanche, a relatively calm period, and a wind event. We analyze maps of snow depth change alongside collected AWS data to pair individual meteorological periods with specific spatial distribution patterns.

To explore the spatial and temporal relationships between elevation, topography, snow depth, and snow depth variability within our study sites we use hypsometric analysis. We calculate the minimum, maximum, mean, median, interquartile range (IQR - the middle 50% of values to reduce the effect of outliers), and coefficient of variation (CV) values for snow depths within each 2 m elevation bin at the Hourglass and Brackett Meadow sites for each collection date. We relate the elevational and temporal results to the terrain features which influence snow depth distributions. We apply this hypsometric analysis to individual sampling day seasonal snow depths and to snow depth changes for each time step between collection dates.

To assess the spatial variability of seasonal snow depth and snow depth change at different scales we calculate CV values within different sized moving windows (López-Moreno et al., 2015). We calculate rasters with circular window diameters of 10, 25, 50, and 100 cm. We explore the scales at which snow depth and snow depth change is spatially variable with different window sizes and observe the locations that frequently exhibit greater variability. We also calculate the mean CV and standard deviation of the CV values for all window sizes at each time step for the Hourglass and Brackett Meadow to identify differences in snow depth and snow depth change variability between the two terrains over the course of the winter.

4. Results

Our findings illustrate the dynamic spatial and temporal snow depth distribution patterns that existed throughout our study areas during the 2019-2020 winter season. We first provide a meteorological overview of the 2019-2020 winter season at the study site in section 4.1. We then discuss potential error in our modeled snow depths in section 4.2. In section 4.3 we examine the relationship between individual meteorological periods and observed spatial distribution patterns. Next, section 4.4 focuses on how elevation and terrain affect the temporal evolution of the total seasonal snow depth and snow depth change. Finally, section 4.5 examines snow depth and snow depth change variability at the slope scale.

4.1 Weather Summary

The 2019-2020 winter in the Bridger Range was distinguished by above average snowfall with a persistent avalanche instability caused by early season snow (Figure 3) (Marienthal, 2020). By late November between 30-50 cm of snow accumulated in areas above 2000 m. Due to strong temperature gradients the snow faceted significantly during intermixed periods of cold dry weather. Steady snowfall during the first half of December was followed by another cold and dry period. Incremental snowfall throughout January resulted in multiple slab avalanches breaking on buried persistent weak layers near the ground throughout the Bridger Range. The most pronounced storm of the season occurred February 1-7, 2020 and deposited ~1 m of snow throughout the region (90 cm at the Brackett Meadow AWS). Consistent storms continued throughout February with another substantial accumulation event (20 cm at Brackett Meadow AWS) occurring

February 25-26, 2020. A natural cornice-triggered deep-slab avalanche in the Hourglass occurred February 26, 2020 near the end of the storm and we were able to collect imagery and a crown profile over the 2 days afterwards (Appendix C Figures 1-3).

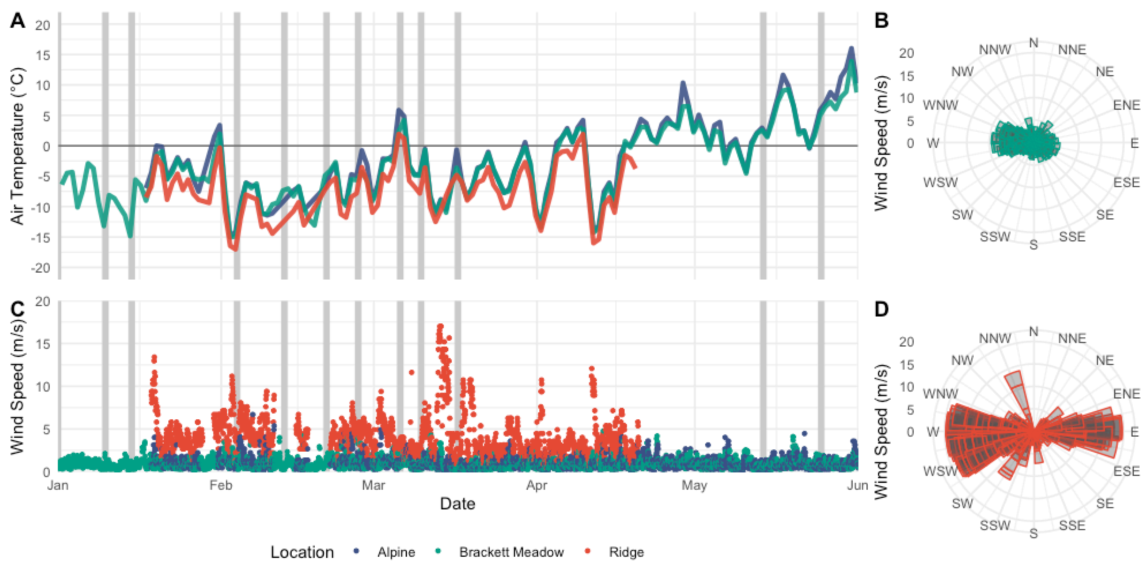

Figure 3: Meteorological summary data from the 2019-2020 winter. (A) Average daily air temperatures (°C), (C) average hourly wind speed (m/s), and average hourly wind speed (m/s) and wind direction for (B) Brackett Meadow and (D) the Ridge. Measurements collected at the AWS in Brackett Meadow (green), the Alpine AWS at Bridger Bowl ski area (purple), and the Ridge AWS at Bridger Bowl ski area (red). Sampling days for UAS-SfM derived snow surface models are marked with grey vertical bars. Additional radiation data can be found in Appendix C Figure 4.

After the avalanche event, warm and dry conditions prevailed through early March with 25 cm of snowpack settlement occurring at Brackett Meadow AWS before a small windy storm March 8, 2020. A substantial and unusual wind event occurred March 13-15, 2020, with sustained 15 m/s easterly winds (as compared to the prevailing westerlies) recorded at Bridger Bowl's Ridge AWS for 48 hours. Gradually warming temperatures and snow accumulation continued throughout the remainder of March, reaching the peak snow depth at Brackett Meadow AWS on April 2, 2020 (242 cm). Aside from a final 30 cm storm April 10-15, 2020, the temperatures continued to warm and remain mostly above freezing while the snowpack ablated through the remainder of our research season.

4.2 Measurement Error

We compare manual in-situ VP and snow survey snow depth measurements (n = 72) with our DSM-differenced snow depths to assess error in our modeled snow depths (Figure 4). We extract the 1 m^2 median and IQR values from the corresponding model for each manually collected snow depth measurement location and use the median value for error assessment. The seasonal mean and standard deviation of differences between modeled and measured snow depths are 16 cm and 73 cm, respectively. The seasonal RMSE and NMAD of differences between modeled and measured snow depths are 74 and 30 cm, respectively. After the removal of outliers greater than 3 standard deviations (n = 2), the seasonal mean, standard deviation and RMSE of differences between modeled and measured snow depths are 7, 51, and 51 cm, respectively, which indicates the outliers' sizable effect on both accuracy and precision. The daily mean, standard deviation, and RMSE of differences between modeled and measured snow depths varied considerably throughout the season (Appendix B Table 2). In addition, daily mean, standard deviation, and RMSE values with the outliers removed show an increase in accuracy and a subtle decrease in precision throughout the season (Appendix C Figure 5).

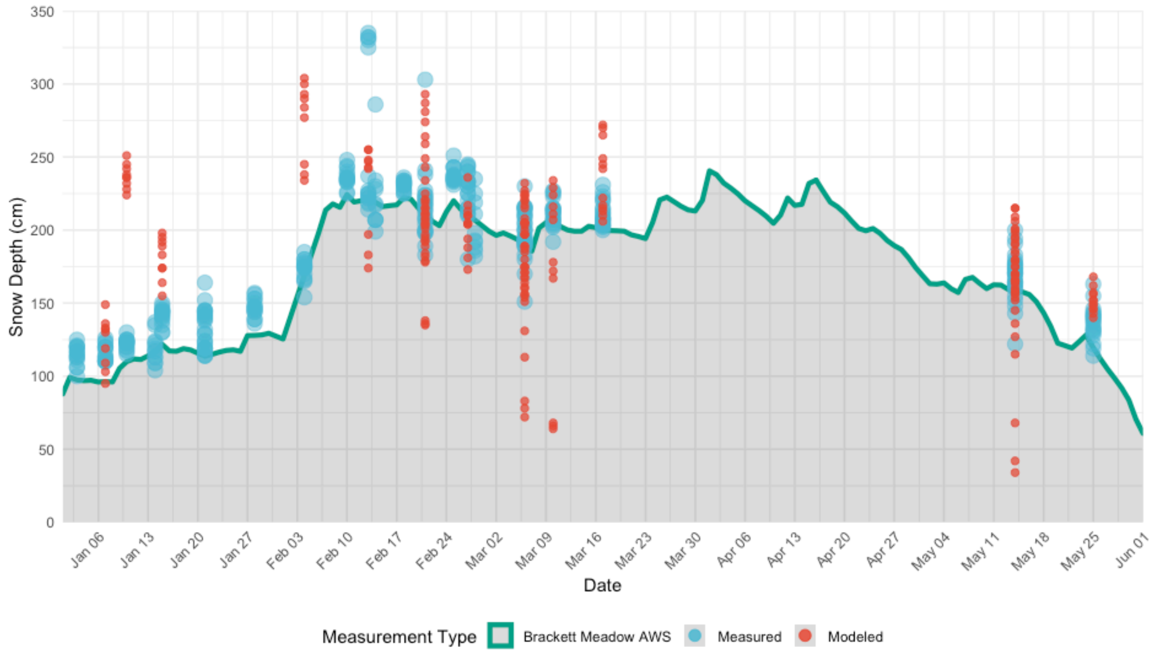

Figure 4: Measured snow depths (cm) from January 1, 2020 - June 1, 2020. "Brackett Meadow AWS" background shading is the sonic-rangefinder measured snow depth at the Brackett Meadow AWS (green line). "Measured" snow depths collected manually in-situ (blue points) are both VPs and snow survey points. "Modeled" points represent DSM-difference derived 1 m^2 quartiles 1, 2 and 3 snow depth measurements (red points). The "Measured" points represent snow depth measurements from within the Bracket Meadow and low relief portions of the Hourglass, and do not represent the same location as the sonic rangefinder attached to the Brackett Meadow AWS.

We collected all of our validation snow depth measurements, except the crown profile of the February 26, 2020 avalanche, in the lower elevations of the Hourglass and throughout Brackett Meadow in order to avoid exposure to snow avalanches. We observed large ranges of measured snow depths within these vegetated areas. For example, the ranges of probed snow depths measured within the 1 m^2 VPs (n = 72) were as high as 49 cm, with an average range of 13 cm. This assessment is not a comprehensive measurement of error because our validation snow depths were primarily collected in the safe lower slopes. Although far from a complete accuracy assessment, our single manual snow depth measurement from upper elevations at the crown of the avalanche exhibited a snow depth difference of only 1.5 cm (190 cm measured vs. 188.5 cm modeled), which is well within the typical error of manual measurement.

4.3 Meteorological Effects on Spatial Snow Depth Change Patterns

To quantify the effect of distinct meteorological periods on snow depth distribution we compared snow depth change maps with meteorological data. We look at four specific events and their unique spatial signatures: the major snow accumulation event in early February, the natural deep slab avalanche on February 26, a period of calm weather in early March, and the sustained easterly wind event in mid-March.

4.3.1 Snow Accumulation Event During the snow accumulation event in early February, there was a non-uniform increase in snow depth throughout the Hourglass and Brackett Meadow (Figure 5). Snow depth change maps show that snow depth change was variable within the upper elevations of the Hourglass (Fig 5A) with pronounced cornice growth along the ridgeline, and pocketed accumulations and redistributions throughout the upper bowl. Below 2420 m, we observe more uniform snow depth increases (Fig 5B). Alternatively, Brackett Meadow shows a non-realistic and an extremely varied pattern with extremely positive (150 cm) and negative (-200 cm) snow depth change values immediately adjacent to each other. We see the largest positive and negative values clearly highlighted by the underlying hillshades: where small trees exist (Fig 5A & 5B) as well as where noisy surface textures resulting from homogenous snow cover are prevalent (Fig 5A & 5C).

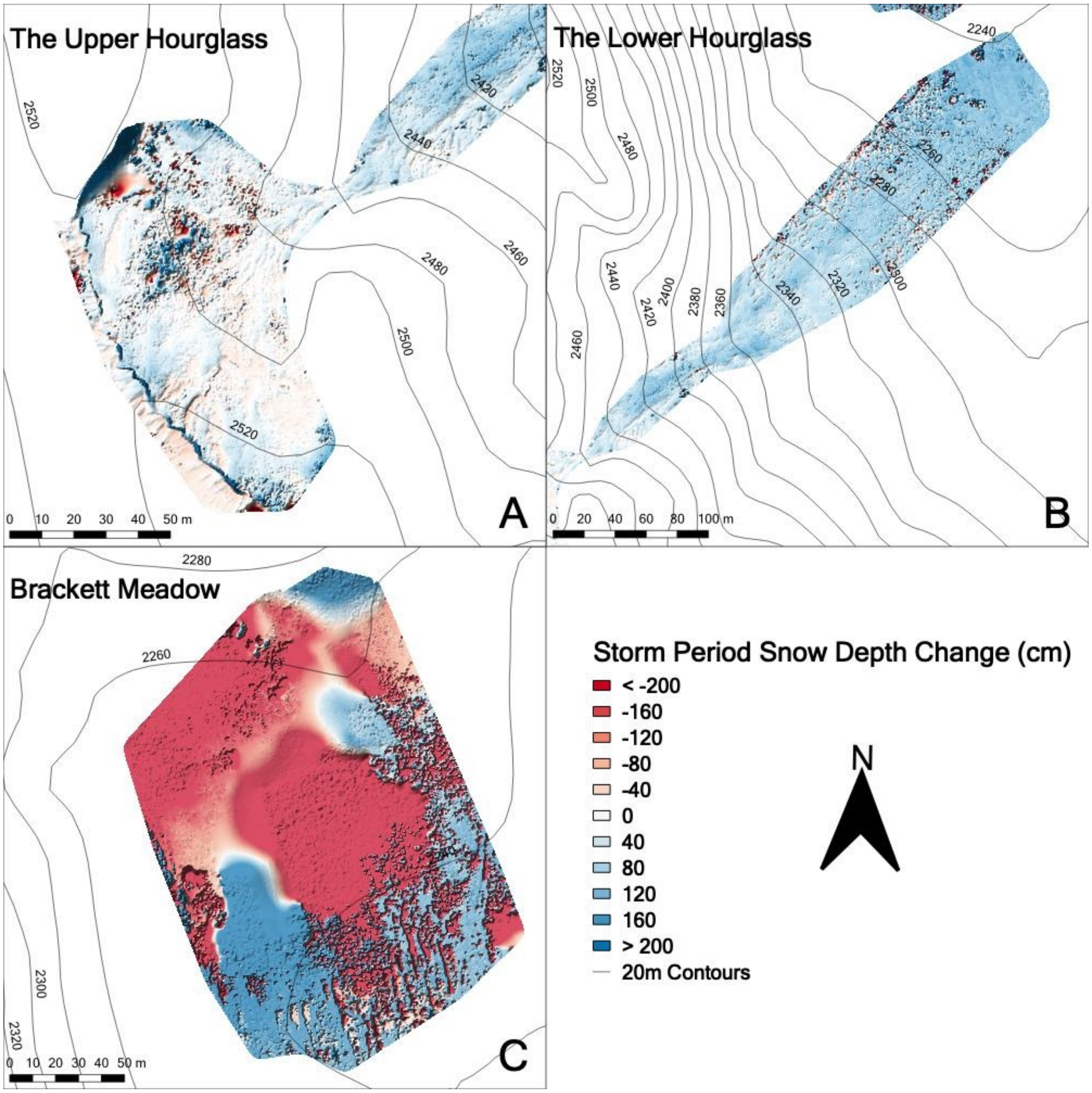

Figure 5: Snow depth change maps of the early February accumulation event. Snow depth change maps depict the January 15 - February 04, 2020 time step. The Hourglass (panels A and B) and Brackett Meadow panel (C) are shown with blue hues indicating snow depth increases, white indicating no change, and red hues indicating snow depth decreases overlaid on hillshades of the DSM surface.

4.3.2 Natural Avalanche Event The February 26, 2020 natural avalanche in the upper elevations of the Hourglass provided a different perspective on snow depth distribution and redistribution. The snow depth change map highlights the disappearance of a section of cornice (dark red), which acted as the trigger for the avalanche, and clearly shows substantial snow loss of 30-190 cm where the slab released (Figure 6). We also see a small increase in snow depth throughout the upper couloir outside of the avalanche area (< 30 cm) and continued cornice growth along the ridgeline (dark blue). We acquired a crown profile at the avalanche's crown line (topmost fracture line) on February 28, 2020 to assess the accuracy of our UAS-derived measurements and found excellent agreement between the manually measured crown height of 190 cm and the UAS-derived height of 188.5 cm.

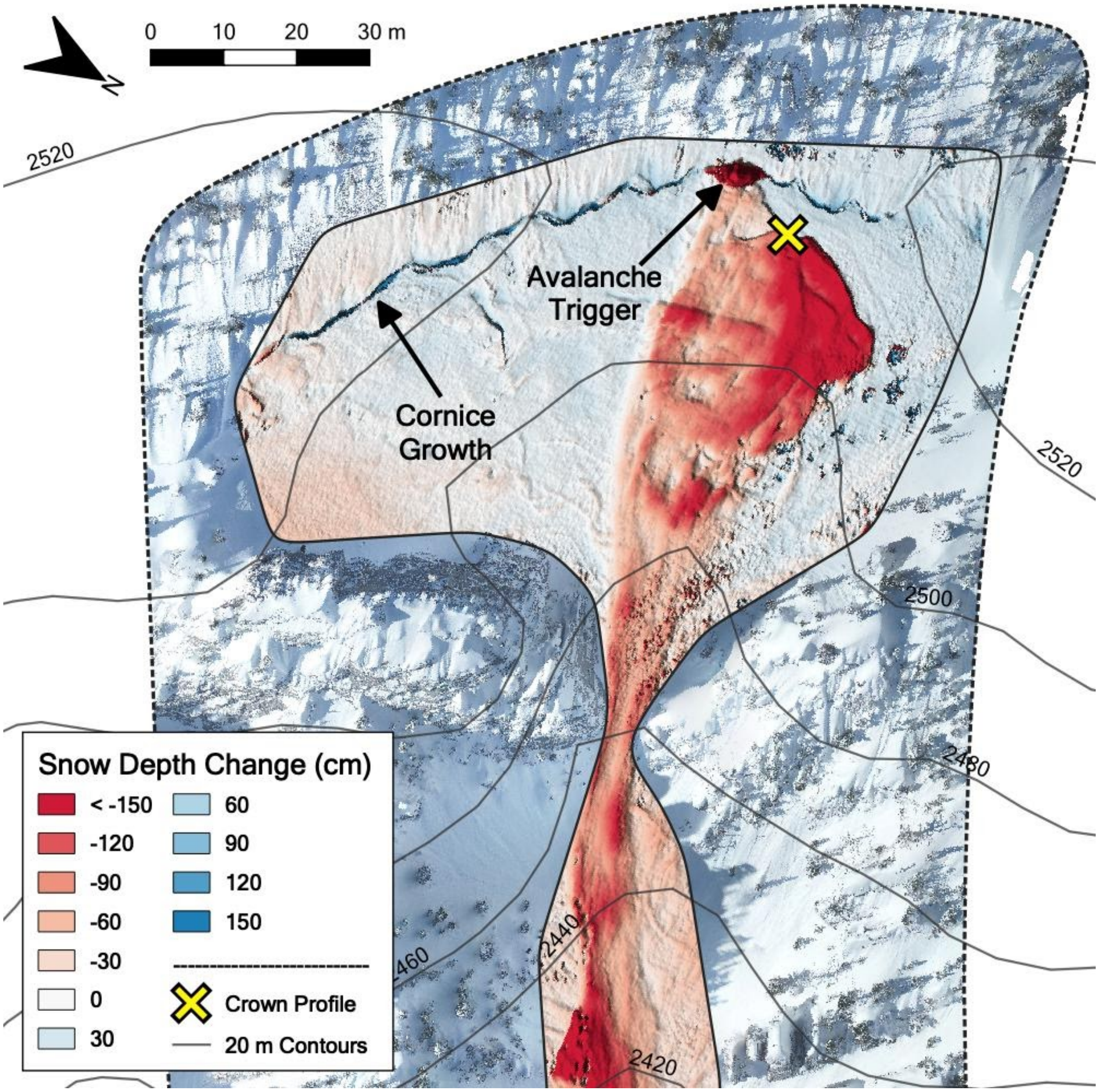

Figure 6: Upper Hourglass snow depth change map post natural avalanche event. The snow depth change map is from the February 21 - 27, 2020 time step overlaid on the February 27, 2020 orthomosaic and hillshade, with 20 m elevation contours shown for reference. The location of the crown profile is marked as a yellow "X" accompanied by arrows denoting the cornice section that fell and triggered the avalanche and continued cornice growth along the ridgeline. The manually collected avalanche crown profile and additional explanatory imagery can be found in Appendix C - Figures 2-4.

Measurements before and after the deep slab avalanche show sizeable snow depth change variability in the avalanched area of the Hourglass with much lower variability outside of the slab boundary (Fig 7A). In the deposition area below, the distinct flowpath of the avalanche debris appears clearly and we observed consistent surface height lowering of ~100 cm throughout the lower elevations of the Hourglass (Fig 7B). Brackett Meadow exhibited a subtle positive to negative gradient in snow depth changes from its northwest to southeast corners (Fig 7C). Extreme positive and negative values of snow depth change were only found around vegetation during this time step (Fig 7B & 7C). Quality surface texture with very little noise, aside from subtle areas of vegetation, appears clearly throughout both the Hourglass and Brackett Meadow sites in the underlying hillshades of this snow depth change time step.

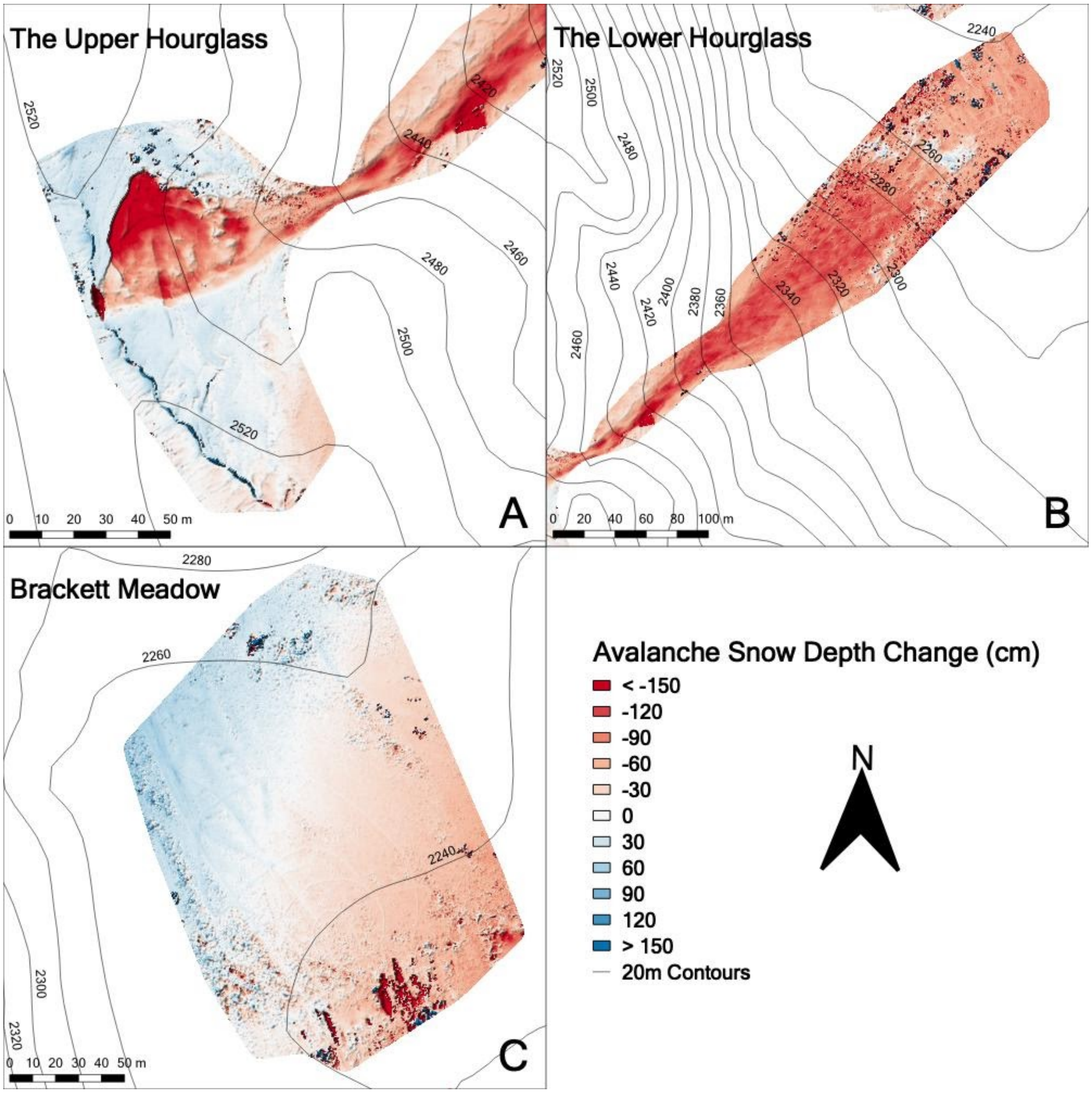

Figure 7: Snow depth change maps of the February 26, 2020 avalanche event. Snow depth change maps depict the February 21 - 27, 2020 time step. The Hourglass (panels A and B) and Brackett Meadow panel (C) are shown with blue hues indicating snow depth increases, white indicating no change, and red hues indicating snow depth decreases overlaid on hillshades of the DSM surfaces.

4.3.3 Calm Weather Period Similar to the snow accumulation event from early February (Figure 6), the Hourglass's upper elevations exhibit more variability in snow depth change than its lower elevations or Brackett Meadow when examining a relatively calm period from February 27 - March 06, 2020. The upper elevations of the Hourglass (Fig 8A) had the greatest snow depth change within the previously avalanched area. Additional small protected pockets below the corniced ridgeline, including the visible previous ski tracks, accumulated 30-60 cm of snow depth during this calm period. During the same time step, most of the cornices observed retreated through ablation or wind stripping. The accumulation of new snow was more pronounced at higher elevations within the Hourglass and tapered to 15 cm or less below 2260 m. Brackett Meadow had a subtle positive to negative snow depth change gradient from its southwest to northeast corners, with unrealistic extreme depths found within trees along its borders.

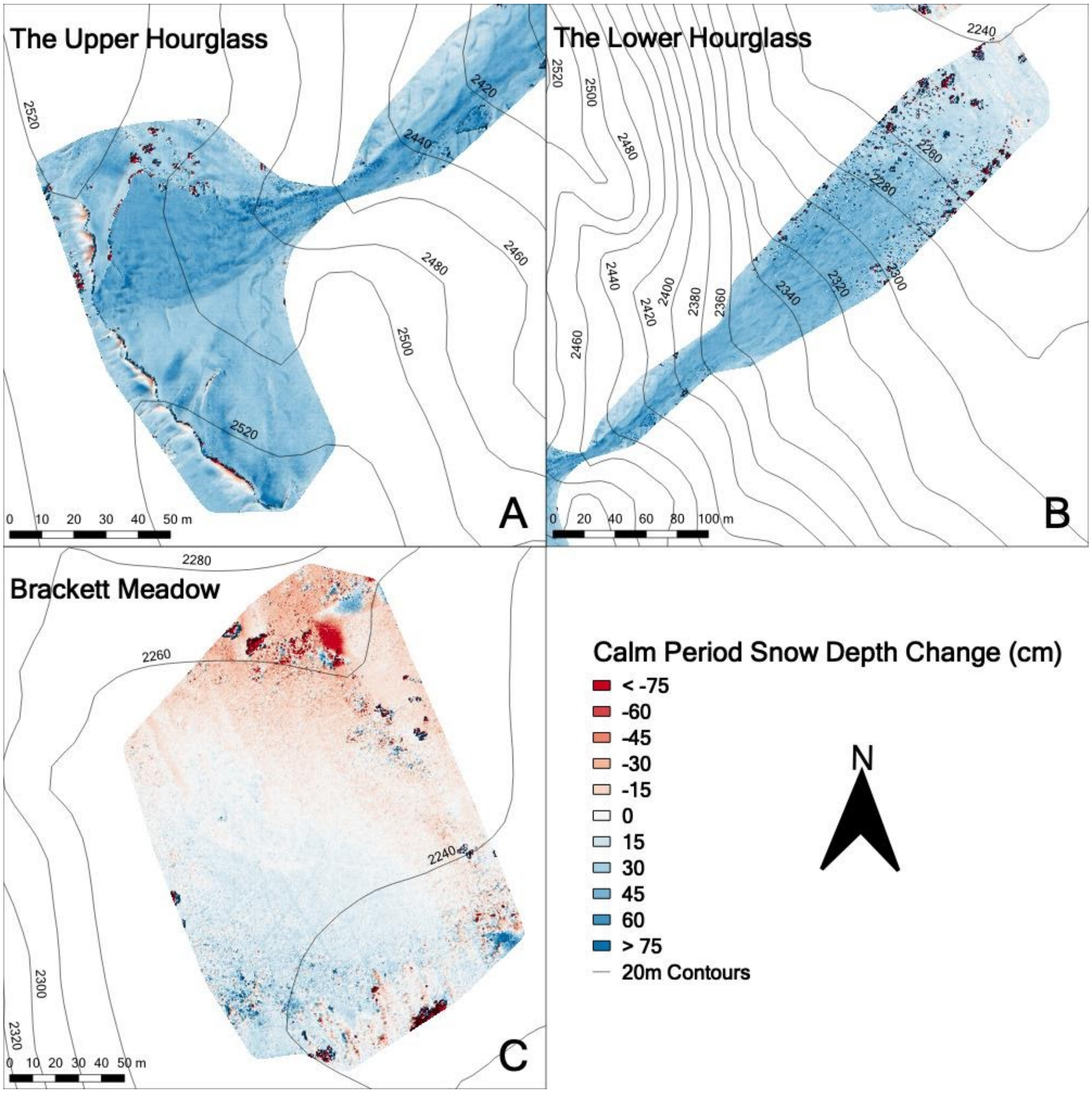

Figure 8: Snow depth change maps of the early March calm period. Snow depth change maps depict the February 27 - March 06, 2020 time step. The Hourglass (panels A and B) and Brackett Meadow panel (C) are shown with blue hues indicating snow depth increases, white indicating no change, and red hues indicating snow depth decreases overlaid on hillshades of the DSM surfaces.

4.3.4 Wind Event Interestingly, the greatest variability among these three non-avalanche weather events exists during the easterly wind event from March 10 - March 17, 2020 (Fig 9). Sizeable snow depth changes exist throughout the Hourglass area (Fig

9A & 9B), with a gradient of negative to positive values from higher to lower elevations. Despite showing non-realistic snow depth changes, there is significantly less snow depth change variability in Brackett Meadow during this period (Fig 9C). This highlights the seasonal differences in wind exposure between the two sites and the effects of wind sheltering on snow redistribution. The elevational snow depth change gradient (Fig 9B) aligns well with increasing protective bordering vegetation along the lower elevations of the Hourglass. The Brackett Meadow AWS generally recorded winds < 5 m/s, while the Ridge AWS regularly measures winds of 5 - 10 m/s throughout the winter (Fig 3C). These ridgetop winds also drive higher magnitude changes near the ridgeline, which result in regular cornice growth throughout the season even though we saw cornice reduction from wind scouring during this easterly wind event. Additionally, the Hourglass ‘s upper and lower elevations exhibit smooth continuous surfaces in the underlying hillshades, resulting in quality modeled snow depths which contrast the noisy Brackett Meadow hillshade and unrealistic modeled snow depths.

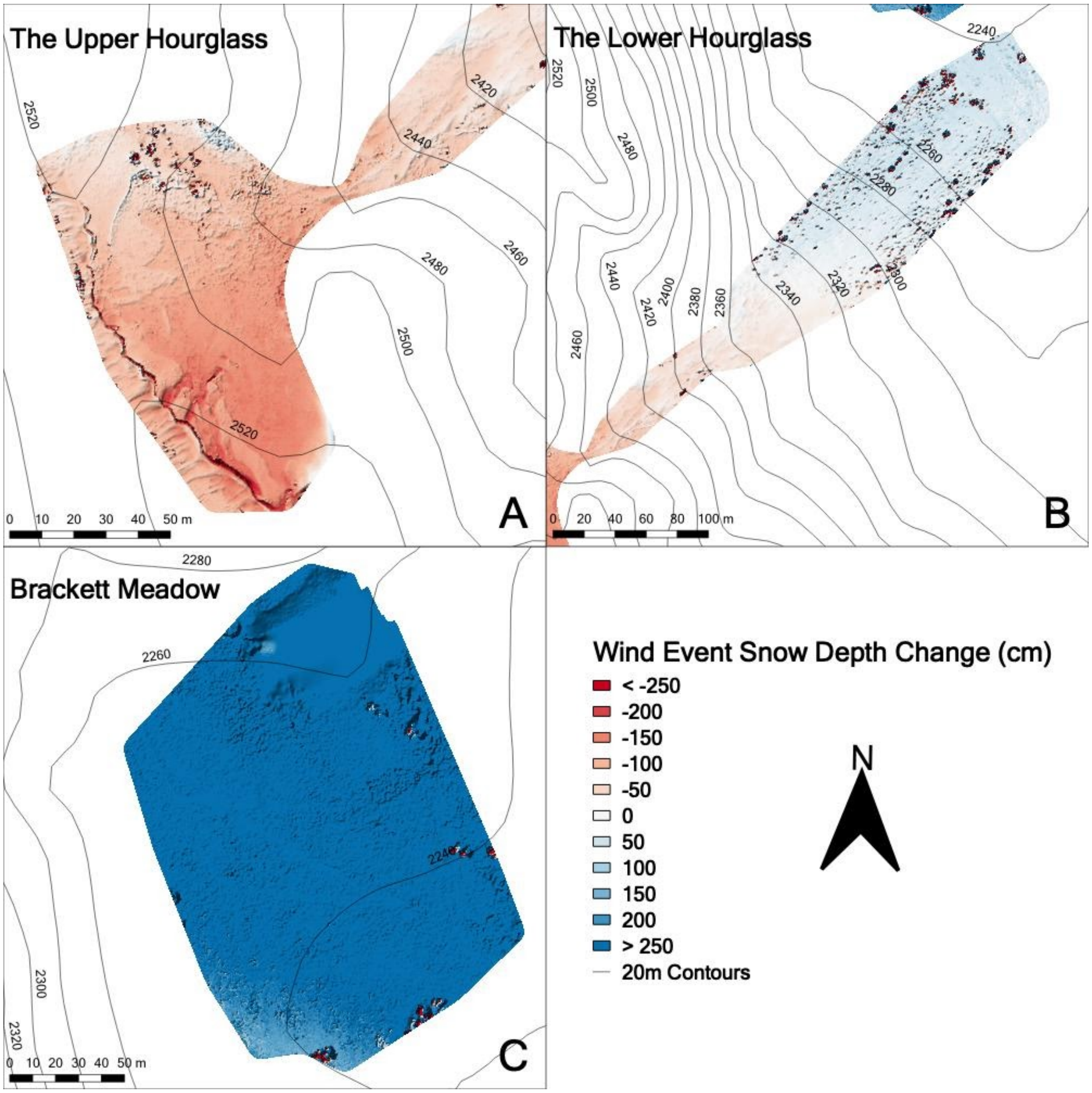

Figure 9: Snow depth change maps of the March 13-15, 2020 easterly wind event. Snow depth change maps are from the March 10 - 17, 2020 time step. The Hourglass (panels A and B) and Brackett Meadow panel (C) are shown with blue hues indicating snow depth increases, white indicating no change, and red hues indicating snow depth decreases overlaid on hillshades of the DSM surfaces.

4.4 Elevation and the Seasonal Evolution of Snow Depth Variability

To explore the spatial and temporal relationships between elevation, snow depth, and snow depth variability within our study sites we use hypsometric analysis. Elevation-binned snow depth distributions are calculated for each individual sampling day as described in Section 3.5. We used median snow depth and IQR values within the 2 m elevation bins in our hypsometric analysis to minimize the effects of outliers from vegetation artifacts in DSM differencing. We found a consistent non-linear pattern with elevation for total snow depth distribution in the Hourglass (Figure 10). We also observed non-uniform accumulation and ablation patterns with elevation. Upon further visual inspection, the most temporally consistent snow depths were found at elevations below 2420 m. The consistently deepest snow depths were between 2350 – 2420 m. We consistently observed the most variability in snow depth in elevation bins above 2420 m (non-shaded areas). Total seasonal snow depths above 2500 m exhibited seasonally-increasing variability as cornices grew along the ridgeline throughout the winter. Below 2260 m, Brackett Meadow occupied proportionally greater surface areas within each elevation bin which resulted in spurious outlier depth values (dark grey shading).

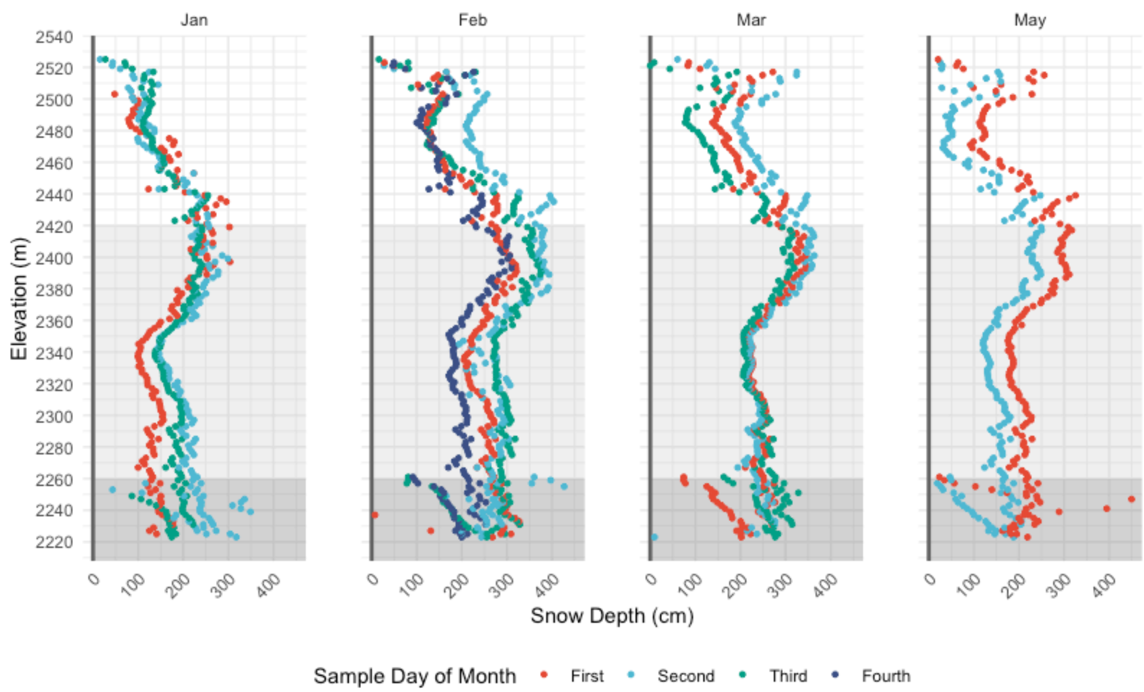

Figure 10: Median hypsometric seasonal snow depths. Values (cm) for the Hourglass derived from 2 m binned elevation bands. Plot panels are divided by the months January, February, March, and May. Discussed elevation zones are depicted in background shading with no shading in the Hourglass upper elevations (> 2420 m), light grey shading in the Hourglass lower elevations (2260 - 2420 m), and dark grey shading in Brackett Meadow elevations (< 2260 m). Points are colored according to their sampling order throughout the month.

Weather events are readily identified in the hypsometric plots of total seasonal snow depth. Sizeable snow depth increase is seen after the early February accumulation event (February panel blue points). The natural slab avalanche on February 26, 2020 is visible in the hypsometric snow depth data collected on February 27, 2020 (February panel purple points), with a distinct decrease in snow depth throughout the Hourglass. This event also influenced subsequent snow depth values collected throughout March by increasing the consistency of snow depth values within the depositional elevation bands (2250 - 2400 m) (March panel). The March 13-15, 2020 easterly wind event appears with sizeable snow depth loss in the upper elevations of the hypsometric plot (March panel green points). May ablation is also observed with uniform snow depth loss throughout all elevations (May panel blue points).

Hypsometric snow depth change distributions were calculated for each individual time step between flight days within the same 2 m elevation bins. The elevation-related accumulation and ablation patterns exhibit a more varied pattern than seasonal snow depth (Figure 11). Observed snow depth changes were more consistent below 2420 m (grey shaded areas) and more variable above this elevation (non-shaded area), similar to the 2 m elevation binned total seasonal snow depth values. The period from February 4 to February 13, 2020 had the greatest observed accumulation with a mean accumulation of 36 cm throughout the Hourglass scene and accumulations of greater than 100 cm above 2420 m (February panel blue points).

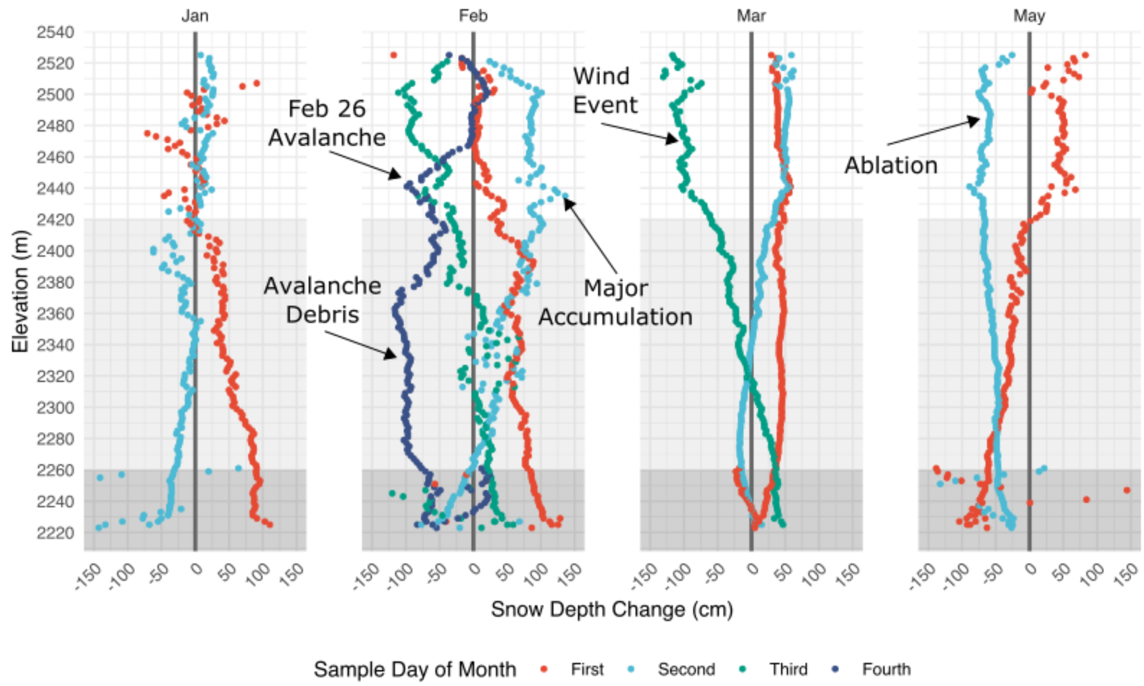

Figure 11: Median hypsometric snow depth change. Values (cm) derived from 2 m binned elevation bands. Plot panels are divided by the months January, February, March, and May. Discussed elevation zones are depicted in background shading with no shading in the Hourglass upper elevations (> 2420 m), light grey shading in the Hourglass lower elevations (2260 - 2420 m), and dark grey shading in Brackett Meadow elevations (< 2260 m). Points are colored according to their sampling order throughout the month.

The natural avalanche event on February 26, 2020 also appears clearly in the snow depth change observed in the February 21-27, 2020 time step (February panel purple points). The mean snow depth change value for this time step is -26 cm between 2440 and 2500 m, the elevation bins where the slab released. Although this value appears low when compared to the 190 cm manually measured avalanche crown height, the avalanche slab only occupied ~25% of the upper elevation bin area. The avalanche affected snow depths occupied proportionally more of the surface area at lower elevations resulting in more negative snow depth change values. The avalanche debris decreased the surface height of the snowpack presumably due to compression and densification of the previous 3 weeks' accumulated low density snow. Within the elevation bins where debris existed (2400 - 2250 m), the mean snow depth change value was -93 cm. In contrast to the slab area, the avalanche debris covered nearly all of the surface area within each of the elevation bins.

The March 13-15, 2020 easterly wind event resulted in a distinct signature in the hypsometric snow depth change signal from March 10-17, 2020 (March panel green points). Our results show a nearly linear gradient of increasingly negative snow depths with increasing elevation, yet small (< 50 cm) accumulation in the more protected lower elevations below 2320 m. Additionally, the results of hypsometric snow depth change of the final time step collected, May 14 - 25, 2020, show a clear pattern of consistent ablation throughout all elevation bands (May panel blue points). Additionally, slightly more negative snow depth change values exist in the elevations where the February 26, 2020 avalanche released from and only the shallow bed surface remained (2440 - 2500 m).

The hypsometric IQR values of snow depth change also exhibit the distinct pattern of high variability earlier in the winter (Figure 12). The consistently highest IQR values of snow depth change (50 - 100 cm) occurred in January, especially at elevations above 2400 m. At elevations from 2300 - 2350 m, the largest IQR values occurred in early February. The consistently lowest IQR values occurred in March, especially in elevations where the February 26, 2020 avalanche debris was deposited (2250 - 2400 m). Brackett Meadow consistently exhibited high snow depth change IQR values throughout the course of the winter, except during late February.

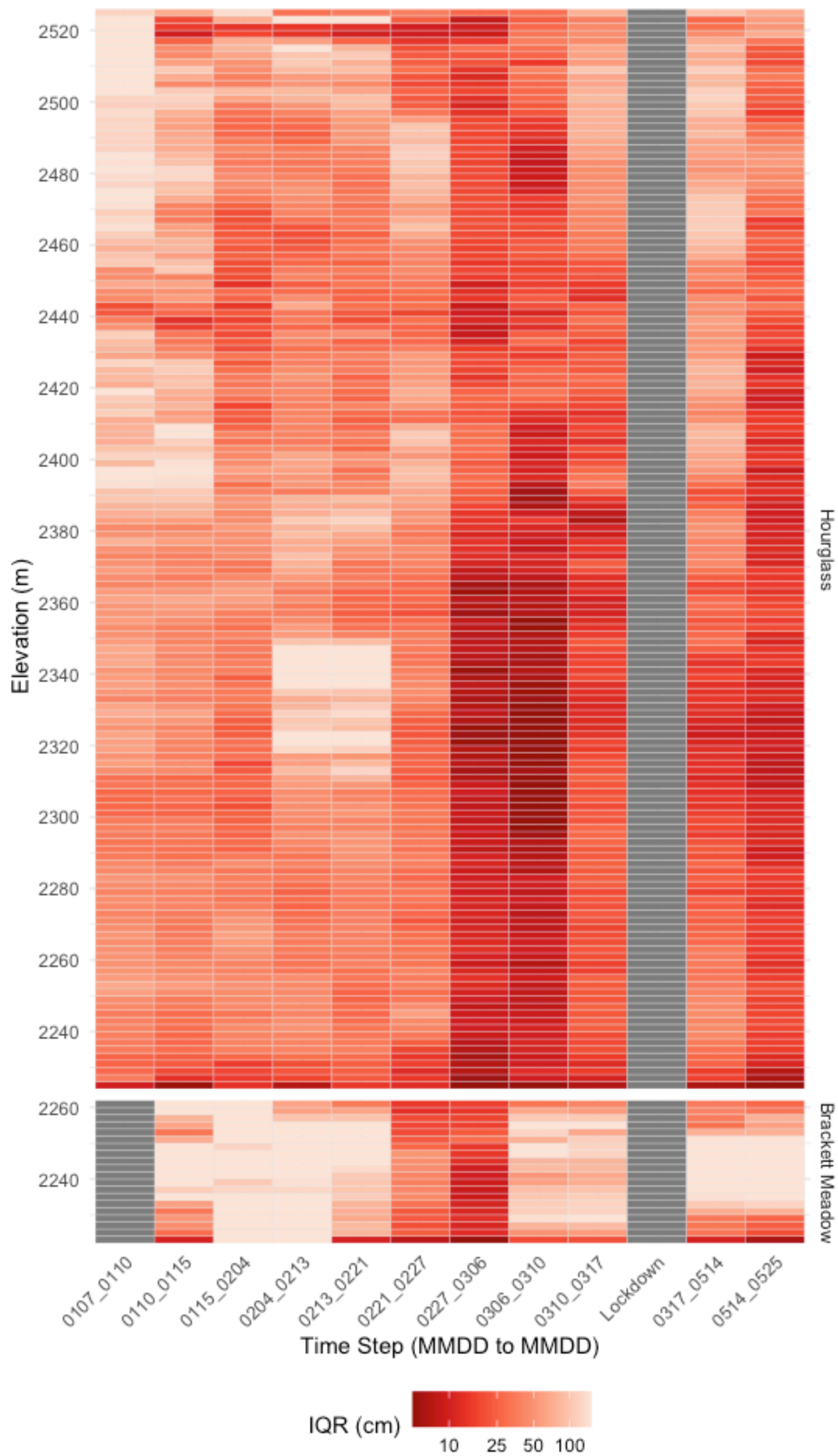

Figure 12: Hypsometric snow depth change absolute IQR values from 2m binned elevation bands. The colors depict absolute IQR values from each 2 m elevation bin (y-axis) for each time step (x-axis) in the Hourglass (top panel) and Brackett Meadow (bottom panel).

4.5 Snow Depth Variability at the Slope Scale

To assess the spatial variability of seasonal snow depth and snow depth change at different scales we calculate CV values within different sized moving windows. We found generally increasing CV values and standard deviation of CV values corresponding to increasing window sizes throughout both the Hourglass and Brackett Meadow (Figure 13 & 14). Additionally, the mean CV and the standard deviation of the CV for total seasonal snow depth and snow depth change is consistently greater for the Hourglass than for Brackett Meadow (Appendix B Table 3). We found that total seasonal snow depths were less spatially variable than snow depth changes. Temporally, both the Hourglass and Brackett Meadow exhibit the most spatial variability early in the season and the least spatial variability in the later season.

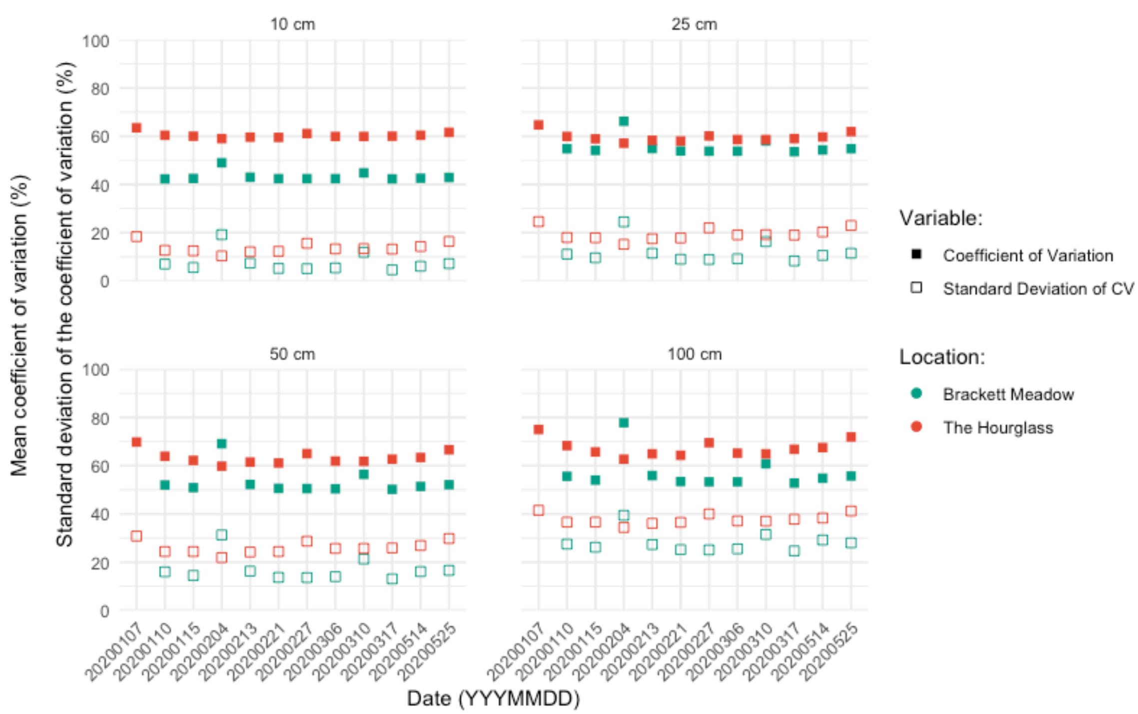

Figure 13: Seasonal snow depth variability. The panels are divided into individual plots for each window scale (10 cm, 25 cm, 50 cm, and 100 cm with CV percentages (solid squares) and the standard deviation (outlined squares) of CV percentages for total

seasonal snow depth on each sampling day from the Hourglass (red) and Brackett Meadow (green).

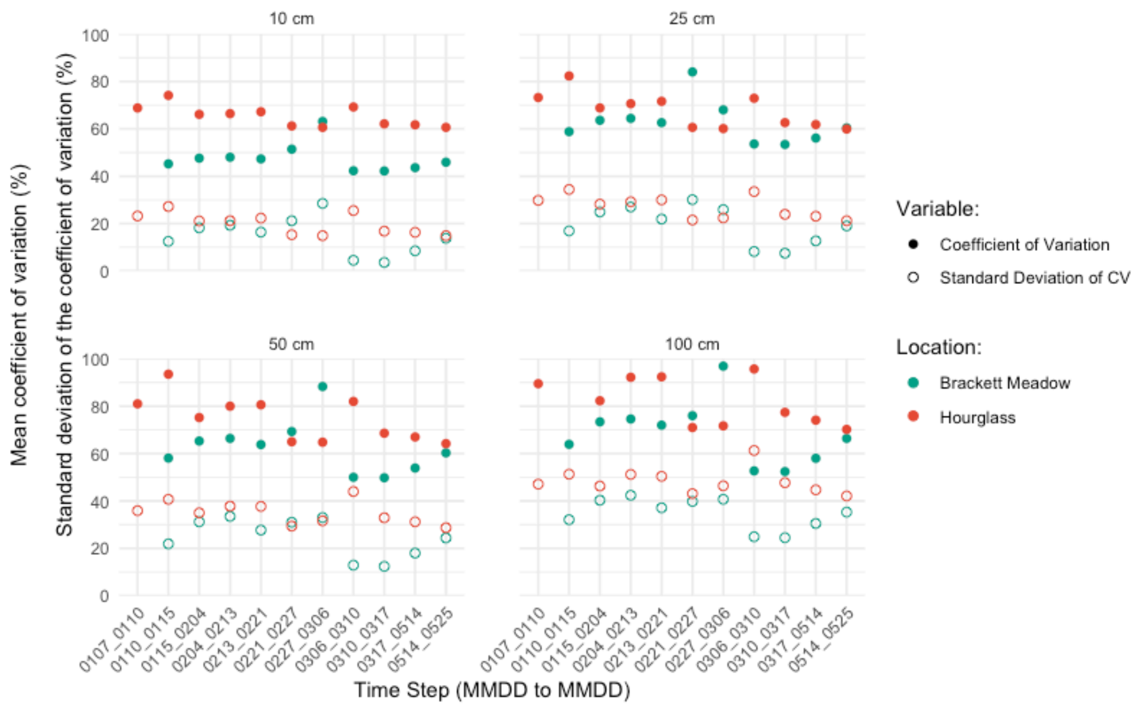

Figure 14: Snow depth change variability. The panels are divided into individual plots for each window scale (10 cm, 25 cm, 50 cm, and 100 cm with CV percentages (solid points) and the standard deviation (outlined points) of CV percentages for snow depth change within each timestep from the Hourglass (red) and Brackett Meadow (green).

Spatially, the Hourglass consistently had the greatest CV values (> 150%) for both snow depth and snow depth change at lower elevations where short trees are spread throughout the slope and can introduce vegetation error in the snow depth measurements (Figure 15). The upper elevations and cornice growth area along the ridgeline of the Hourglass exhibit consistently greater snow depth and snow depth change CV values. The consistently largest snow depth change CV values (~100%) in Brackett Meadow were along its southern flank (Figure 15). Brackett Meadow has lower seasonal mean CV values than the Hourglass for total seasonal snow depth and snow depth change (57% and

69% vs. 67% and 84%, respectively). Seasonal snow depth change was more variable than total seasonal snow depths for the Hourglass and Brackett Meadow by 17% and 12%, respectively.

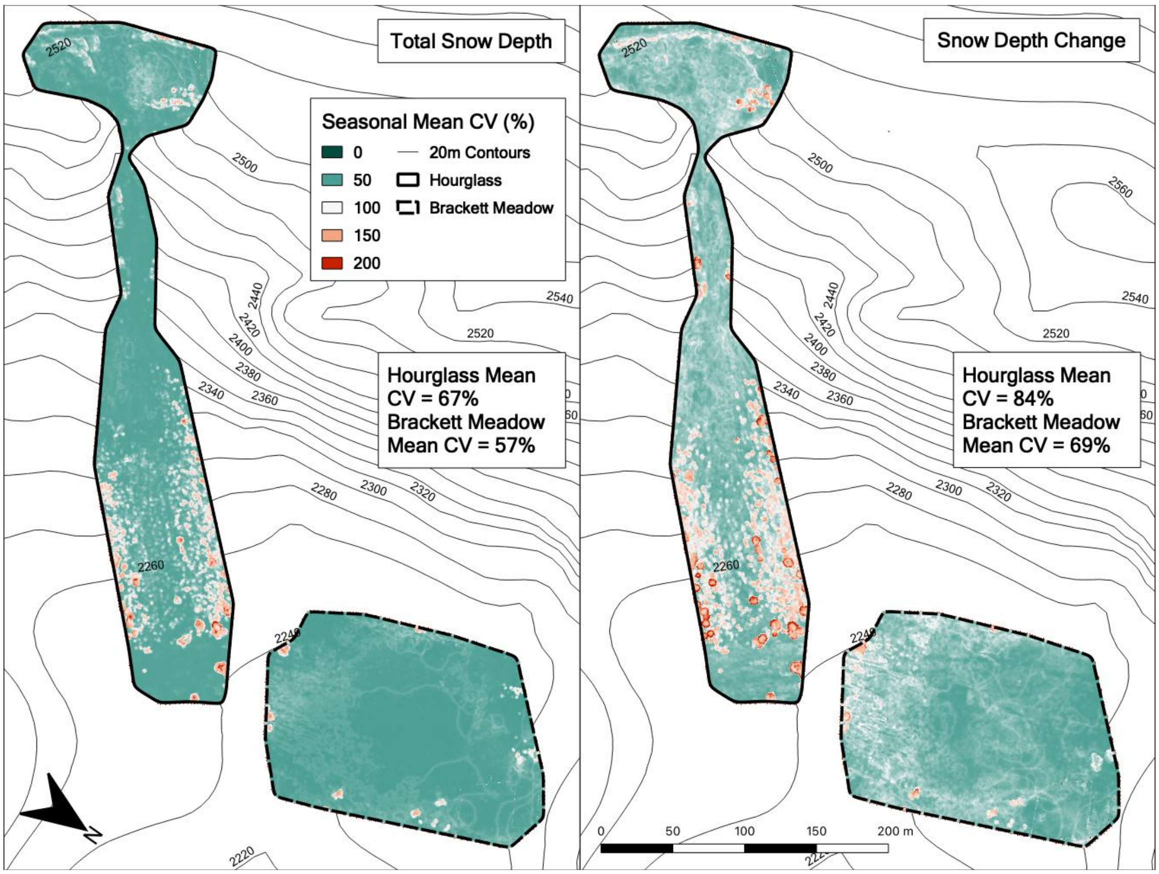

Figure 15: Seasonal mean coefficient of variation map of the Hourglass and Brackett Meadow. CV values (%) are shown as a gradient from 0% (green) to 100% (white) to 200% (red) and represent the mean value of each cell from the collection of all 100 cm window total snow depth and snow depth change CV rasters.

For individual time step maps of snow depth change CV, the decimeter scale window size highlights specific centimeter-scale areas of increased variability, but are much harder for interpreting slope-scale spatial trends (Figure 16). As the window scale increases, so does the variability observed. Within the 50 cm window size, trends such as cornice growth begin to appear more clearly (Fig 16C). At the 100 cm window size, spatial variability is most pronounced yet also obscures some of the finer scale features (Fig 16D).

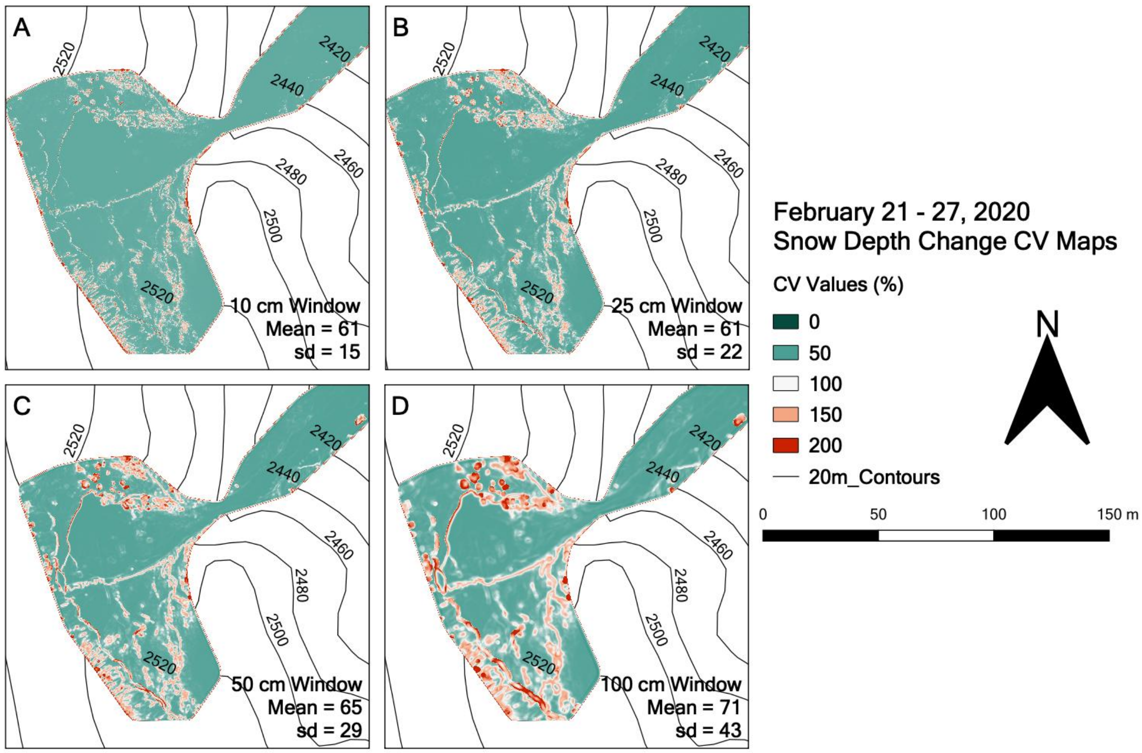

Figure 16: Snow depth change coefficient of variation maps. Panels denote individual window sizes for the calculation of CV values surrounding each pixel of the Hourglass for the February 21 - 27, 2020 timestep. Window sizes of (A) 10 cm , (B) 25 cm, (C) 50 cm, and (D) 100 cm each show the mean and standard deviation (sd) values of the CV maps.

5. Discussion

Our study analyzes slope-scale spatial and temporal snow depth variability in adjacent steep and flat mountain terrain using snow depth maps derived from UAS-SfM photogrammetry collected over 13 days throughout the winter and spring of 2019 - 2020. We compare the 2x2 cm resolution snow depth maps in sequence to examine the spatial and temporal evolution and variability of mountain snowpacks. We use these datasets to quantify the spatial and temporal variability of snow depths at the slope scale, to explore the interactions between snow depth distribution and several specific weather and avalanche events, to compare variability in different mountain terrain, and to observe patterns of variability at a variety of scales.

5.1 Measurement Error

Our results reinforce the effectiveness of a UAS-SfM workflow for measuring the spatial variability of snow depths at centimeter scale in complex terrain. The calculated RMSE from our combined flights is greater than reported in previous research, but the daily RMSE had significant range related to individual sampling day's conditions and resultant model quality (Appendix B Table 2). Our daily RMSE values aligned with previously reported findings by Bühler et al. (2016) (< 15 cm on rocks and < 30 cm on grass), De Michelle et al. (2016) (14 cm), Lendzioch et al. (2016) (22 cm in open spaces and 42 cm in forested areas), Harder et al. (2016) (between 8.5 cm and 13.7 cm), Avanzi et al. (2017) (17 to 31 cm depending on filtering), and Cimoli et al. (2017) (4.6 to 18.6 cm over a variety of ground covers). One key difference from previous studies is that our study collected the majority of our validation snow depth measurements in areas with considerable observable vegetation.

A common source of uncertainty in DSM differenced snow depth measurement is the handling of vegetation (De Michelle et al., 2016). The lower elevations of the Hourglass and entire Brackett Meadow areas are densely covered with 10 - 150 cm vegetation (grasses and small shrubs) that can vary more than 50 cm in height over less than 50 cm distances. These features move in the wind, compress differently under the snowpack, support variable snow deposition on their branches, and occupy proportionally less surface area as the snow accumulates and buries them. These dynamic changes result in different possible DSM-differenced measurements of snow depth (Adams et al., 2018 and Bühler et al., 2016). Furthermore, tall coniferous trees created unrealistic snow depths in some instances. Tall trees sway in the wind resulting in subtle misalignments between co-registered models and extreme DSM-differenced snow depth outliers. Agisoft Metashape often struggles to resolve tie points within dynamic vegetation that can change during the course of a single 10 - 15 minute flight.

Homogeneous surfaces with little visual texture also produce outlier snow depth data because they limit the ability of SfM software to find matching tie points (Bühler et al., 2017). We frequently observed very little surface texture within the Brackett Meadow site due to its wind sheltered location. Modeled surfaces with processing artifacts resulted from these homogenous areas and are clearly seen in the underlying hillshades of Brackett Meadow (Figures 6 - 9). There was a clear improvement in modeled surface quality near ski tracks or with older snow surfaces. Our noisy modeled surfaces closely resemble those discussed in Bühler et al. (2017), where they used near-infrared imagery to improve the surface texture and, consequently, tie point recognition of homogenous snow surfaces. Consequently, we see high IQR values and unrealistic snow depth change values from this uncertainty within the Brackett Meadow site. In contrast, we frequently observed substantial surface texture in the Hourglass due to wind redistribution, wind deposition of vegetative debris and loose dry snow sloughing. This texture resulted in better modeled surfaces and realistic snow depths.

Therefore, we focus on median and quartile values to assess snow depth measurements in our hypsometric analysis to limit the effects of extreme outlier values resulting from vegetation effects and artifacts of homogenous snow surfaces similar to those described in Cimoli et al. (2017) and Meyer et al. (2021). We did not mask out or remove these extreme outlier snow depths because cornice growth similarly presents as large outliers but provides important information for understanding snow depth change variability within the slope scale.

Our manual measurements followed traditional and accepted techniques, but collecting validation snow depth measurements throughout the entire Hourglass scene was generally not possible due to an unacceptable level of risk. However, our single validation measurement in the upper elevations exhibited only 1.5 cm of difference between the model and avalanche crown profile (Figure 7). Although one measurement is not sufficient to thoroughly assess model accuracy in this region, this result provides some confidence that the model performs similarly well across the study area.

5.2 Meteorological Effects on Spatial Snow Depth Change Patterns

To quantify the effect of distinct meteorological periods on spatial snow depth distribution we compared the snow depth change maps and coincidental meteorological data of four specific meteorological periods. There are many factors that led to differences in snow depth changes and variability between the different topographies of the Hourglass and Brackett Meadow sites. A full analysis of topographic feature interactions with micro-meteorological patterns is outside of the scope of this paper, but the following cursory discussion of logical interactions between terrain and weather serves as a path for future work.

During storm events, the Hourglass received more snow due to consistent wind-loading and depositions from predominantly westerly-flows aligning nearly perpendicular to the Bridger Range ridgeline (Birkeland, 2001; Lundy et al., 2001). The upper elevations of the Hourglass experienced greater snow depth and snow depth change spatial variability, probably due to its increased exposure to ridgetop winds as well as the micro terrain and wind eddy interactions within the upper bowl. This finding aligns with those of Wirz et al. (2011) which emphasized wind's interactions with spatial and temporal distributions of snow depth in steep terrain. These interactions and resultant snow deposition patterns must be influenced by the near-vertical 30 m cliff along the southeastern edge and its connected constriction confining the terminus of the upper bowl. At mid-elevations below the constriction (2460 m), storm period snow depth changes were more gradual and can probably be attributed to frequent sluffing and small snow avalanches depositing debris from the steeper upper bowl. Additionally, the steep slopes surrounding these mid-elevations sheltered the slope and resulted in noticeably less wind effect throughout the season, with the exception of this topography acting as a funnel for upslope easterly winds as seen in snow depth decreases from the March 13 - 15, 2020 easterly wind event.

On the other hand, Brackett Meadow experienced very little additional wind deposition during storm events because it lies 300 m below the ridgeline and is well sheltered from winds with forested hillslopes to its north and south and steep rock cliffs to its west. Consequently, snow depth in Brackett Meadow increased and decreased generally uniformly during different meteorological periods.

The avalanche event resulted in an unexpected surface lowering within the deposition area and throughout the lower elevations of the Hourglass (Figure 7B). This lowering may be the result of rapid settling and consolidation of the recent low density snowfall between our previous flight date (February 21, 2020) and the post-avalanche flight date (February 27, 2020), and from additional consolidation of the storm snow by the much more dense avalanche debris. During the same period, the Brackett Meadow AWS experienced settlement rates of 5 - 10 cm/day. This finding is more pronounced than Prokop et al. (2015), who found a subtle surface lowering through much of the deposition area, although not all of it, when mapping an artificially triggered snow avalanche using TLS, total station, and photogrammetric methods.

During meteorological periods favoring steady or decreasing snow depth, changes in the upper elevations of the Hourglass remained spatially variable as winds frequently redistributed loose snow, grew cornices, and solar input melted snow on its south and southeastern aspects. These steep terrain-related findings are similar to the terrain influenced findings of Wirz et al. (2011) who mapped snow depth on a steep rock face throughout a season using terrestrial laser scanning. The February 27 – March 6, 2020 calm period and the March 13 - 15, 2020 easterly wind event highlight the dynamic nature of spatial variability within the Hourglass by exhibiting non-uniform patterns of snow depth accumulation and reduction especially in the upper elevations (> 2450 m). The preferential refilling then scouring of the previously avalanched area of the

Hourglass is especially relevant for our understanding of snow distributions in complex, avalanche effected terrain in the mountains. The temporal signature of the avalanche on snow depth distributions, therefore, is much greater than the event itself. This finding encourages further exploration of the seasonal effects of these events on mountain snow distributions because of the resultant effects on runoff timing with more variable snow depths at higher elevations which tend to melt out the latest.

During these same meteorological periods, Brackett Meadow's snow depth change spatial variability increased but to a much lesser degree than the Hourglass. This variability in Brackett Meadow was presumably due largely to direct solar inputs and subsequent ablation. This is apparent in the consistently increased variability along the southern flank of Brackett Meadow, where tall coniferous trees preferentially shade the southern edge of the site for much of the winter and intermittent sunshine between trees create spatially variable patterns in snow depth change.

If locations such as Brackett Meadow are where snow water equivalent is traditionally quantified, the differences in spatial distribution patterns of snow depth discussed here suggest a need for further research on the snow distribution differences between steep complex terrain and typical snow depth measurement sites. Analyzing spatial snow depth changes and coincidentally collected meteorological data at the Hourglass and Brackett Meadow study sites further illustrate the necessity for research on the effects of interactions between topography and micro-meteorology on snow distribution in complex mountain terrain.

5.3 Elevation and the Seasonal Evolution of Snow Depth Variability

To explore the spatial and temporal relationships between elevation, snow depth, and snow depth variability within our study sites we use hypsometric analysis. The Hourglass consistently displayed more variability in snow depth change than Brackett Meadow, but the range of variability within the Hourglass showed a decreasing trend throughout the season (Figure 12). This may be due to seasonally increasing total snow depths creating more uniform surfaces on which snow depth changes are less affected by small terrain features or vegetation. Total snow depths gradually grew throughout both sites, but became especially consistent in the Hourglass after the natural avalanche event (Figure 10). Within the avalanche debris deposition elevations (2250 - 2400 m) the compaction and densification of the previous three week's accumulation of low density surface snow resulted in increasing homogeneity for the remainder of the season. Alternatively, in the elevations where the avalanche slab released, we continued to see greater variability for the remainder of the season.

Temporal variability in snow depth change distributions appeared more gradually in Brackett Meadow. It's sheltered and nearly flat position within the surrounding terrain essentially eliminated the effects of wind redistribution, natural avalanches and sloughing of new snow. Thus, temporal and spatial snow depth changes and snow depth variability were directly related to storm specific accumulation amounts while increasing in snow depth and exposure to warm temperatures and direct sunlight while ablating.

Our results suggest shorter temporal processes such as avalanches and wind redistribution effect the spatial variability of the Hourglass more than longer term processes such as radiation driven ablation. Changes on longer timescales, such as ablation driven by increasing temperatures and solar radiation, have more of an effect on the spatial variability of Brackett Meadow. These differences in the temporal scales of snow depth variability are apparent in the differences between our two compared terrains.

We found a non-uniform distribution of snow depth and non-linear increases in total snow depth with elevation throughout our two sites (Figure 10). This is similar to the slope scale findings of Grünewald et al. (2014), where the deepest snow depths were found in the depositional areas below the steepest slopes normally associated with upper elevations. Throughout the entire season, we consistently observed the deepest total snow depths in the Hourglass's mid-elevations (2350 - 2450 m). These deep depositions primarily result from natural sloughing of loose dry snow from steep terrain above into the protected shallow slopes below. These deep areas may also be contributed to snow redistributed from wind exposed upper elevations into slightly lower more sheltered mid elevations. Alternatively, the lower elevations of the Hourglass displayed relatively consistent snow depth accumulation, ablation, and measured variability (IQR), which aligns well with our expectation of the lower slope angled, vegetated and sheltered portion of the slope.

Our hypsometric analysis was less effective at capturing the true variability and accurate aggregated snow depth information for Brackett Meadow than the Hourglass during our study. Brackett Meadow has much less relief than the Hourglass, yet its surface area within each 2 m elevation bin is much larger. These larger areas provided considerably more measurements per elevation bin and, in combination with previously discussed inaccurate homogenous snow surface models within the sheltered meadow, resulted in very large measures of IQR throughout the season. This implied variability in snow depths and snow depth changes is generally not in agreement with the in-situ manually measured variability observed throughout Brackett Meadow. Brackett Meadow showed consistently lower spatial variability in snow depth change when compared with the Hourglass over the course of the season when quality surface models were produced.

Elevation varied total snow depths indicate the dynamic nature of snow depth and snow depth change variability within steeper more complex mountain terrain (Figure 11 & 12). These elevation derived findings illustrate the need for further investigations of terrain specific interactions with snow depth distributions.

5.4 Snow Depth Variability at the Slope Scale

To address the question of snow depth variability spatial resolutions we calculate total snow depth and snow depth change coefficient of variation values within different sized moving windows. The results of this research confirm the high degree of spatial variability of snow depths reported in previous studies from snow hydrology and snow avalanche research fields. López-Moreno et al. (2015) noted that the mean CV increased with increasing spatial scales (from 5x5 m to 99x99 m square windows), which is in agreement with our findings at much finer scales (10 cm to 100 cm diameter circle windows). López Moreno et al. also found the lowest variability in deeper snowpacks, which we also observed with lower mean seasonal CV values for total snow depth in the deepest areas of the Hourglass (Figure 15). Kronholm and Birkeland (2007) explored the effects of sampling designs in slope scale snow surveys and found consistent sample variogram lag ranges between 5.23 and 5.74 m. Their findings suggest that there is greater consistency within sampling distances of ~5.5 m than sampling at greater distances, and they found CV values for those ranges of 14 - 28%. In contrast, with a 1 m moving window the Hourglass and Brackett Meadow's seasonal mean snow depth CV values were 67% and 57%, respectively, and their mean snow depth change CV values were 84% and 69%, respectively. Thus, our seasonal snow depths and snow depth changes displayed greater variability than expected of a sampling snow survey at finer than 1 m spatial resolution. We attempted to complete a 5 m diameter moving window calculation of CV throughout our site to compare to Kronholm and Birkeland (2007) and López-Moreno et al. (2015), but lacked sufficient computational resources to complete it. Wirz et al. (2011) found similarly widely varying CV values for snow depth change (-343% to 242%) with a 1 m spatial resolution during their study of snow depth evolution on steep rock faces and also reported higher spatial variability in total snow depths in steeper complex terrain when compared to gentle nearby slopes.

Mendoza et al. (2020) found CV values varied (60% to > 100%) in their 25 m elevation binned snow depths with larger values at higher elevations and in more forested areas. This is in agreement with our finding of the greatest CV values being in vegetated areas within our study site. They also found smaller semi-variogram scale breaks (~4 m) in vegetation dominated topographies, reinforcing our sub 1 m model resolution decisions for complex sub-alpine slope scale analysis. We attempted a semi-variogram analysis to explore scale-breaks occurring within our two sites, but lacked sufficient computational resources to complete it. Our finer scale focus examined incremental snow depth change questions within the slope scale and, consequently, we saw a greater connection between our resultant CV values and shorter time-frame individual meteorological events.

Examining the snow depth CV change maps from the February 21 - 27, 2020 timestep illustrates the interactions of scale and observed variability more clearly (Figure 16). The 10 cm window size (Fig 16A) subtly highlights the edges of the avalanche crown face and flanks (edges of slab release area), as well as faintly showing ski tracks of a searching party and continued cornice growth. The 50 cm window (Fig 16C) clearly highlights all the mentioned features and still maintains their sharp boundaries. The 100 cm window size (Fig 16D) further highlights areas of increased variability. Within our current window size computational limitations, the 100 cm window effectively captures snow depth and snow depth variability at the slope scale in complex sub-alpine mountain terrain. Using similar methods to acquire high resolution snow depth data, further exploration of the scales of spatial variability should focused on specific process scales, such as avalanche formation or wind redistribution, to improve our understanding of these distributions within the slope scale and to improve data collection efficiency of future work.

5.5 Limitations and Future Work

Assessing snow depth variability in rugged mountain terrain presents a variety of environmental challenges. Traditional methods, such as probing, expose field workers to cold temperatures and are frequently spatially limited to areas without significant avalanche hazard. Gaffey and Bhardwaj (2020) describe the utility of UAS for snow depth measurement in sub-watershed scale areas that are challenging or unsafe to access and require high resolution mapping. Utilizing UAS to collect photos for photogrammetric surface processing allows field workers to avoid exposure to avalanches and creates a spatially continuous dataset, but introduces additional environmental limitations. Our flights were limited by strong ridgetop winds, frequent cloud cover, intermittent precipitation, cold temperatures, and field site accessibility. Although modern UAS are becoming more capable, these extreme conditions can cause instrument error and failure resulting in inaccurate data collection or no data collection. We must be aware of these environmental limitations for future operational use.

An example of these limitations is apparent in our UAS data collected on January 21, 2020. The resultant surface heights of this model show a snow surface lower than that of the snow-free July 8, 2020 model surface (below ground level) at lower elevations in the study site. The 291 cm difference between the mean measured snow depth (142 cm) and the mean modeled snow depth (-149 cm) is due to extremely poor photo location information despite PPK processing, caused by uncorrectable RTK locational errors. Since these equipment malfunctions are possible when operating in winter conditions, the resultant DSMs still require human interpretation to assess accuracy.

Whether utilizing UAS for further snow distribution research or operational avalanche implementation, the environmental limitations and common conditions at a potential field site should be considered. The use of alternative sensors such as near-infrared cameras or lidar-equipped UAS, that are less susceptible to low light and homogenous snow surfaces within the visual light spectrum, is an obvious direction for improving surface measurement, but can come at a significant cost increase (Deems et al., 2016; Bühler et. al, 2017). To further constrain snow depth measurement error in steep mountainous terrain, future studies should consider the addition of fixed snow depth stakes distributed throughout the study site to act as reference datums. The unfortunate reality at our study location is that installing fixed snow depth stakes with sufficient height (3 m for the Hourglass) that resist snowpack creep and avalanches while not interfering with public recreational users was not feasible.

Considering the interactions of complex terrain and snow depth variability, it seems prudent to leverage the opportunity to map snow surfaces at high resolution to further explore additional topographic features of high-mountain terrain to continue to build our understanding of how and where snow is deposited for both the avalanche hazard and water resource fields. UAS and SfM photogrammetry continue to prove to be an effective tool in mapping snow surfaces in steep complex dynamic mountain terrain.

6. Conclusion

This research uses a time series of 13 UAS-derived 2 cm resolution snow surface models to map the evolution of and quantify snow depth and snow depth change spatial variability within the slope scale. We focus on steep complex mountain terrain and compare our results to an adjacent low relief meadow to observe spatial patterns of snow distributions over the course of the 2019 - 2020 winter and validate our results with traditional manual in-situ measurements. We successfully used UAS and SfM photogrammetry techniques to collect and model the snow surface in a variety of winter conditions. We achieved comparable results to previous studies which focused on less heterogeneous terrain and demonstrated the utility of UAS and SfM photogrammetry for relatively low cost, high resolution mapping of snow depths in mountainous terrain. Using these data, we quantified the evolution of seasonal snow depths of up to 3 m throughout a 300 m couloir and an adjacent mountain meadow.

As expected, our research found distinct patterns of spatial snow depth change corresponding to specific meteorological events. We compared meteorological data collected in the immediate vicinity of the study site with snow depth change maps to assess for spatial and temporal patterns in snow depth change variability. We identified and quantified specific patterns of spatial variability for a storm event depositing approximately 1 m of snow, a natural snow avalanche event, a relatively calm weather period, and a strong sustained wind event. With the exception of the surface lowering from the natural avalanche debris deposition and unrealistic meadow results due to homogenous snow surfaces, our results demonstrated the expected effects of weather's interactions with topography. Each of these natural events, as well as increasing or decreasing snow depth conditions in between, presented its own unique signature of the spatial variability of snow depth change.

Similar to other research, our study revealed a non-linear and non-uniform relationship between snow accumulation and elevation at our study site. We used hypsometric analysis for each sampling day to track the total seasonal snow depth evolution as well as between days to assess elevation-related patterns in snow depth change. We found the greatest snow depths at mid-elevations (2350 - 2420 m) below the steeper upper elevations of our terrain. Our results suggest seasonal trends in snow depth variability that fluctuate with elevation. As expected, higher elevations earlier in the season had the greatest variability within our study site due to their exposure to wind and steeper slope angles which naturally slough and avalanche redistributing snow more frequently. We also observed a general decrease in variability throughout the winter season throughout all elevations of our study sites.

This study aligns with previous snow depth variability work, finding that measures of variability tend to increase with increasing window size, at least to the 100 cm resolution tested. Although scales of > 100 cm are sufficient for total snow depth variability (De Michelle et al. 2016), our work shows the relevance of higher spatial resolution mapping for tracking individual storm influence and snow accumulation spatial distributions. Our specific focus on snow depth change results in a further understanding of scale effects of snow depth variability within the sub 100 cm scale.

REFERENCES CITED

Adams, M., Bühler, Y., & Fromm, R. (2018). Multitemporal Accuracy and Precision Assessment of Unmanned Aerial System Photogrammetry for Slope-Scale Snow Depth Maps in Alpine Terrain. Pageoph, 175(9), 3303–3324. https://doi.org/10.1007/s00024-017-1748-y

Agisoft. (2020). AgiSoft PhotoScan Professional (Version 1.6.2). http://www.agisoft.com/downloads/installer/

Alidoost, F., & Arefi, H. (2017). COMPARISON OF UAS-BASED PHOTOGRAMMETRY SOFTWARE FOR 3D POINT CLOUD GENERATION: A SURVEY OVER A HISTORICAL SITE. ISPRS Annals of Photogrammetry, Remote Sensing and Spatial Information Sciences, IV-4/W4, 55–61. https://doi.org/10.5194/isprs-annals-IV-4-W4-55-2017

Anderton, S. P., White, S. M., & Alvera, B. (2004). Evaluation of spatial variability in snow water equivalent for a high mountain catchment. Hydrological Processes, 18(3), 435–453. https://doi.org/10.1002/hyp.1319

Avanzi, F., Bianchi, A., Cina, A., De Michele, C., Maschio, P., Pagliari, D., Passoni, D., Pinto, L., Piras, M., & Rossi, L. (2017). Measuring the snowpack depth with Unmanned Aerial System photogrammetry: Comparison with manual probing and a 3D laser scanning over a sample plot. The Cryosphere Discussions, 1–19. https://doi.org/10.5194/tc-2017-57

Avanzi, F., De Michele, C., Morin, S., Carmagnola, C. M., Ghezzi, A., & Lejeune, Y. (2016). Model complexity and data requirements in snow hydrology: Seeking a balance in practical applications: Complexity versus data requirements in snow hydrology models. Hydrological Processes, 30(13), 2106–2118. https://doi.org/10.1002/hyp.10782

Birkeland, K. W. (2001). Spatial patterns of snow stability throughout a small mountain range. Journal of Glaciology, 47(157), 176–186. https://doi.org/10.3189/172756501781832250

Birkeland, Karl W., Johnson, R. F., & Schmidt, D. S. (1998). Near-Surface Faceted Crystals Formed by Diurnal Recrystallization: A Case Study of Weak Layer Formation in the Mountain Snowpack and Its Contribution to Snow Avalanches. Arctic and Alpine Research, 30(2), 200. https://doi.org/10.2307/1552135

Birkeland, Karl W., & Mock, C. J. (1996). Atmospheric Circulation Patterns Associated with Heavy Snowfall Events, Bridger Bowl, Montana, U.S.A. Mountain Research and Development, 16(3), 281–286. https://doi.org/10.2307/3673951

Birkeland, K. W., Hansen, K. J., & Brown, R. L. (1995). The spatial variability of snow resistance on potential avalanche slopes. *Journal of Glaciology*, *41*(137), 183–190. https://doi.org/10.3189/S0022143000017871

Blöschl, G., & Sivapalan, M. (1995). Scale issues in hydrological modelling: A review. Hydrological Processes, 9(3–4), 251–290. https://doi.org/10.1002/hyp.3360090305

Blöschl, Günter. (1999). Scaling issues in snow hydrology. Hydrological Processes, 13(14–15), 2149–2175. https://doi.org/10.1002/(SICI)1099-1085(199910)13:14/15<2149::AID-HYP847>3.0.CO;2-8

Bösch, R., Bühler, Y., Marty, M., & Ginzler, C. (2016). COMPARISON OF DIGITAL SURFACE MODELS FOR SNOW DEPTH MAPPING WITH UAV AND AERIAL CAMERAS. ISPRS - International Archives of the Photogrammetry, Remote Sensing and Spatial Information Sciences, XLI-B8, 453–458. https://doi.org/10.5194/isprsarchives-XLI-B8-453-2016

Brandt, W. T., Bormann, K. J., Cannon, F., Deems, J. S., Painter, T. H., Steinhoff, D. F., & Dozier, J. (2020). Quantifying the Spatial Variability of a Snowstorm Using Differential Airborne Lidar. Water Resources Research, 56(3). https://doi.org/10.1029/2019WR025331

Bühler, Y., Marty, M., Egli, L., Veitinger, J., Jonas, T., Thee, P., & Ginzler, C. (2015). Snow depth mapping in high-alpine catchments using digital photogrammetry. The Cryosphere, 9(1), 229–243. https://doi.org/10.5194/tc-9-229-2015

Bühler, Yves, Adams, M. S., Bösch, R., & Stoffel, A. (2016). Mapping snow depth in alpine terrain with unmanned aerial systems (UASs): Potential and limitations. The Cryosphere, 10(3), 1075–1088. https://doi.org/10.5194/tc-10-1075-2016

Bühler, Yves, Adams, M. S., Stoffel, A., & Bösch, R. (2017). Photogrammetric reconstruction of homogenous snow surfaces in alpine terrain applying near-infrared UAS imagery. International Journal of Remote Sensing, 38(8–10), 3135–3158. https://doi.org/10.1080/01431161.2016.1275060

Carbonneau, P. E., & Dietrich, J. T. (2017). Cost-effective non-metric photogrammetry from consumer-grade sUAS: Implications for direct georeferencing of structure from motion photogrammetry. Earth Surface Processes and Landforms, 42(3), 473–486. https://doi.org/10.1002/esp.4012

Cimoli, E., Marcer, M., Vandecrux, B., Bøggild, C. E., Williams, G., & Simonsen, S. B. (2017). Application of Low-Cost UASs and Digital Photogrammetry for High-Resolution Snow Depth Mapping in the Arctic. Remote Sensing, 9(11), 1144. https://doi.org/10.3390/rs9111144

Clark, M. P., Hendrikx, J., Slater, A. G., Kavetski, D., Anderson, B., Cullen, N. J., Kerr, T., Örn Hreinsson, E., & Woods, R. A. (2011). Representing spatial variability of snow water equivalent in hydrologic and land-surface models: A review: REPRESENTING SPATIAL VARIABILITY OF SWE IN MODELS. Water Resources Research, 47(7). https://doi.org/10.1029/2011WR010745

Colomina, I., & Molina, P. (2014). Unmanned aerial systems for photogrammetry and remote sensing: A review. ISPRS Journal of Photogrammetry and Remote Sensing, 92, 79–97. https://doi.org/10.1016/j.isprsjprs.2014.02.013

Conway, H., Abrahamson, J., & Young, R. (1986). A Field Test to Assess Snow-Slope Stability. Journal of Glaciology, 32(112), 535–537. https://doi.org/10.3189/S0022143000012260

Currier, W. R., Pflug, J., Mazzotti, G., Jonas, T., Deems, J. S., Bormann, K. J., Painter, T. H., Hiemstra, C. A., Gelvin, A., Uhlmann, Z., Spaete, L., Glenn, N. F., & Lundquist, J. D. (2019). Comparing Aerial Lidar Observations With Terrestrial Lidar and Snow-Probe Transects From NASA's 2017 SnowEx Campaign. Water Resources Research, 55(7), 6285–6294. https://doi.org/10.1029/2018WR024533

De Michele, C., Avanzi, F., Passoni, D., Barzaghi, R., Pinto, L., Dosso, P., Ghezzi, A., Gianatti, R., & Della Vedova, G. (2016). Using a fixed-wing UAS to map snow depth distribution: An evaluation at peak accumulation. The Cryosphere, 10(2), 511–522. https://doi.org/10.5194/tc-10-511-2016

Deems, J. S. (2002). Topographic effects on the spatial and temporal patterns of snow temperature gradients in a mountain snowpack [Montana State University]. https://scholarworks.montana.edu/xmlui/handle/1/8287

Deems, J. S., Painter, T. H., & Finnegan, D. C. (2013). Lidar measurement of snow depth: A review. Journal of Glaciology, 59(215), 467–479. https://doi.org/10.3189/2013JoG12J154

Dozier, J. (2011). Mountain hydrology, snow color, and the fourth paradigm. Eos, Transactions American Geophysical Union, 92(43), 373–374. https://doi.org/10.1029/2011EO430001

Dozier, J., Bair, E. H., & Davis, R. E. (2016). Estimating the spatial distribution of snow water equivalent in the world's mountains. WIREs Water, 3(3), 461–474. https://doi.org/10.1002/wat2.1140

Eberhard, L. A., Sirguey, P., Miller, A., Marty, M., Schindler, K., Stoffel, A., & Bühler, Y. (2021). Intercomparison of photogrammetric platforms for spatially continuous snow depth mapping. The Cryosphere, 15(1), 69–94. https://doi.org/10.5194/tc-15-69-2021

Egli, L., Griessinger, N., & Jonas, T. (2011). Seasonal development of spatial snow-depth variability across different scales in the Swiss Alps. Annals of Glaciology, 52(58), 216–222. https://doi.org/10.3189/172756411797252211

Elder, K., Rosenthal, W., & Davis, R. E. (1998). Estimating the spatial distribution of snow water equivalence in a montane watershed. HYDROLOGICAL PROCESSES, 12, 16.

Fierz, C., R.L, A., Y, D., P, E., Greene, E., Mcclung, D., Nishimura, K., Satyawali, P., & Sokratov, S. (2009). The international classification for seasonal snow on the ground (UNESCO, IHP (International Hydrological Programme)–VII, Technical Documents in Hydrology, No 83; IACS (International Association of Cryospheric Sciences) contribution No 1).

Gabrlik, P., Janata, P., Zalud, L., & Harcarik, J. (2019). Towards Automatic UAS-Based Snow-Field Monitoring for Microclimate Research. Sensors, 19(8), 1945. https://doi.org/10.3390/s19081945

Gaffey, C., & Bhardwaj, A. (2020). Applications of Unmanned Aerial Vehicles in Cryosphere: Latest Advances and Prospects. Remote Sensing, 12(6), 948. https://doi.org/10.3390/rs12060948

Gillan, B. J., Harper, J. T., & Moore, J. N. (2010). Timing of present and future snowmelt from high elevations in northwest Montana. Water Resources Research, 46(1). https://doi.org/10.1029/2009WR007861

Goetz, J., & Brenning, A. (2019). Quantifying Uncertainties in Snow Depth Mapping From Structure From Motion Photogrammetry in an Alpine Area. Water Resources Research, 55(9), 7772–7783. https://doi.org/10.1029/2019WR025251

Greene, E., Birkeland, K. W., Kelly, E., McCammon, I., Staples, M., & Sharaf, D. (2016). Snow, Weather, and Avalanches: Observation Guidelines for Avalanche Programs in the United States (D. Krause, Ed.; 3rd ed.). American Avalanche Association.

Grünewald, T., Bühler, Y., & Lehning, M. (2014). Elevation dependency of mountain snow depth. The Cryosphere, 8(6), 2381–2394. https://doi.org/10.5194/tc-8-2381-2014

Hägeli, P., & McClung, D. M. (2004). Hierarchy theory as a conceptual framework for scale issues in avalanche forecast modeling. Annals of Glaciology, 38, 209–214. https://doi.org/10.3189/172756404781815266

Hanzer, F., Helfricht, K., Marke, T., & Strasser, U. (2016). Multilevel spatiotemporal validation of snow/ice mass balance and runoff modeling in glacierized catchments. The Cryosphere, 10(4), 1859–1881. https://doi.org/10.5194/tc-10-1859-2016

Harder, P., Schirmer, M., Pomeroy, J., & Helgason, W. (2016). Accuracy of snow depth estimation in mountain and prairie environments by an unmanned aerial vehicle. The Cryosphere, 10(6), 2559–2571. https://doi.org/10.5194/tc-10-2559-2016

Hendrikx, J., Birkeland, K., & Clark, M. (2009). Assessing changes in the spatial variability of the snowpack fracture propagation propensity over time. Cold Regions Science and Technology, 56(2–3), 152–160. https://doi.org/10.1016/j.coldregions.2008.12.001

Höhle, J., & Höhle, M. (2009). Accuracy assessment of digital elevation models by means of robust statistical methods. ISPRS Journal of Photogrammetry and Remote Sensing, 64(4), 398–406. https://doi.org/10.1016/j.isprsjprs.2009.02.003

Hu, F., Gao, X. M., Li, G. Y., & Li, M. (2016). DEM EXTRACTION FROM WORLDVIEW-3 STEREO-IMAGES AND ACCURACY EVALUATION. ISPRS - International Archives of the Photogrammetry, Remote Sensing and Spatial Information Sciences, XLI-B1, 327–332. https://doi.org/10.5194/isprsarchives-XLI-B1-327-2016

Jamieson, J. B., & Johnston, C. D. (1992). Snowpack characteristics associated with avalanche accidents. Canadian Geotechnical Journal, 29(5), 862–866. https://doi.org/10.1139/t92-093

Kinar, N. J., & Pomeroy, J. W. (2015). Measurement of the physical properties of the snowpack: MEASUREMENT OF SNOWPACK. Reviews of Geophysics, 53(2), 481–544. https://doi.org/10.1002/2015RG000481

Kronholm, K., & Birkeland, K. W. (2005). Integrating spatial patterns into a snow avalanche cellular automata model: SNOW AVALANCHE CELLULAR AUTOMATA MODEL. Geophysical Research Letters, 32(19), n/a-n/a. https://doi.org/10.1029/2005GL024373

Kronholm, K., & Birkeland, K. W. (2007). Reliability of sampling designs for spatial snow surveys. Computers & Geosciences, 33(9), 1097–1110. https://doi.org/10.1016/j.cageo.2006.10.004

Kronholm, K., & Schweizer, J. (2003). Snow stability variation on small slopes. Cold Regions Science and Technology, 37(3), 453–465. https://doi.org/10.1016/S0165-232X(03)00084-3

LaChapelle, E. R. (1980). The Fundamental Processes in Conventional Alavalanche Forecasting. Journal of Glaciology, 26(94), 75–84. https://doi.org/10.3189/S0022143000010601

Landry, C., Birkeland, K., Hansen, K., Borkowski, J., Brown, R., & Aspinall, R. (2004). Variations in snow strength and stability on uniform slopes. Cold Regions Science and Technology, 39(2–3), 205–218. https://doi.org/10.1016/j.coldregions.2003.12.003

Lehning, M., Bartelt, P., Brown, B., Russi, T., Stöckli, U., & Zimmerli, M. (1999). Snowpack model calculations for avalanche warning based upon a new network of weather and snow stations. Cold Regions Science and Technology, 30(1–3), 145–157. https://doi.org/10.1016/S0165-232X(99)00022-1

Lendzioch, T., Langhammer, J., & Jenicek, M. (2016). TRACKING FOREST AND OPEN AREA EFFECTS ON SNOW ACCUMULATION BY UNMANNED AERIAL VEHICLE PHOTOGRAMMETRY. ISPRS - International Archives of the Photogrammetry, Remote Sensing and Spatial Information Sciences, XLI-B1, 917–923. https://doi.org/10.5194/isprsarchives-XLI-B1-917-2016

Liston, G. E., & Elder, K. (2006). A Distributed Snow-Evolution Modeling System (SnowModel). Journal of Hydrometeorology, 7(6), 1259–1276. https://doi.org/10.1175/JHM548.1

Logan, S., Birkeland, K., Kronholm, K., & Hansen, K. (2007). Temporal changes in the slope–scale spatial variability of the shear strength of buried surface hoar layers. Cold Regions Science and Technology, 47(1–2), 148–158. https://doi.org/10.1016/j.coldregions.2006.08.002

López-Moreno, J. I., Revuelto, J., Fassnacht, S. R., Azorín-Molina, C., Vicente-Serrano, S. M., Morán-Tejeda, E., & Sexstone, G. A. (2015). Snowpack variability across various spatio-temporal resolutions. Hydrological Processes, 29(6), 1213–1224. https://doi.org/10.1002/hyp.10245

Lundy, C. C., Brown, R. L., Adams, E. E., Birkeland, K. W., & Lehning, M. (2001). A statistical validation of the snowpack model in a Montana climate. Cold Regions Science and Technology, 33(2–3), 237–246. https://doi.org/10.1016/S0165-232X(01)00038-6

Lutz, E. R., & Birkeland, K. W. (2011). Spatial patterns of surface hoar properties and incoming radiation on an inclined forest opening. Journal of Glaciology, 57(202), 355–366. https://doi.org/10.3189/002214311796405843

Marienthal, A. (2020). GNFAC 2019-2020 snowpack summary. Gallatin National Forest Avalanche Center. https://www.mtavalanche.com/sites/default/files/2020-04/GNFAC%2019-20%20snowpack%20summary.pdf

Marti, R., Gascoin, S., Berthier, E., de Pinel, M., Houet, T., & Laffly, D. (2016). Mapping snow depth in open alpine terrain from stereo satellite imagery. The Cryosphere, 10(4), 1361–1380. https://doi.org/10.5194/tc-10-1361-2016

McClung, D. M., & Schaerer, P. (2006). The Avalanche Handbook (3rd Edition). The Mountaineers, Seattle, WA.

McCormack, E., & Vaa, T. (2019). Testing Unmanned Aircraft for Roadside Snow Avalanche Monitoring. Transportation Research Record: Journal of the Transportation Research Board, 2673(2), 94–103. https://doi.org/10.1177/0361198119827935

Mendoza, P. A., Musselman, K. N., Revuelto, J., Deems, J. S., López-Moreno, J. I., & McPhee, J. (2020). Interannual and Seasonal Variability of Snow Depth Scaling Behavior in a Subalpine Catchment. Water Resources Research, 56(7). https://doi.org/10.1029/2020WR027343

Mendoza, P. A., Shaw, T. E., McPhee, J., Musselman, K. N., Revuelto, J., & MacDonell, S. (2020). Spatial Distribution and Scaling Properties of Lidar-Derived Snow Depth in the Extratropical Andes. Water Resources Research, 56(12). https://doi.org/10.1029/2020WR028480

Meyer, J., & Skiles, S. M. (2019). Assessing the Ability of Structure From Motion to Map High-Resolution Snow Surface Elevations in Complex Terrain: A Case Study From Senator Beck Basin, CO. Water Resources Research, 2018WR024518. https://doi.org/10.1029/2018WR024518

Meyer, J., Skiles, S. M., Deems, J., Bormann, K., & Shean, D. (2021). Mapping snow depth and volume at the alpine watershed scale from aerial imagery using Structure from Motion [Preprint]. Snow/Remote Sensing. https://doi.org/10.5194/tc-2021-34

Mock, C. J., & Birkeland, K. W. (2000). Snow Avalanche Climatology of the Western United States Mountain Ranges. Bulletin of the American Meteorological Society, 81(10), 2367–2392. https://doi.org/10.1175/1520-0477(2000)081<2367:SACOTW>2.3.CO;2

Molotch, N. P., & Bales, R. C. (2006). SNOTEL representativeness in the Rio Grande headwaters on the basis of physiographics and remotely sensed snow cover persistence. Hydrological Processes, 20(4), 723–739. https://doi.org/10.1002/hyp.6128

Nolan, M., Larsen, C. F., & Sturm, M. (2015). Mapping snow-depth from manned-aircraft on landscape scales at centimeter resolution using Structure-from-Motion photogrammetry. The Cryosphere Discussions, 9(1), 333–381. https://doi.org/10.5194/tcd-9-333-2015

Painter, T. H., Berisford, D. F., Boardman, J. W., Bormann, K. J., Deems, J. S., Gehrke, F., Hedrick, A., Joyce, M., Laidlaw, R., Marks, D., Mattmann, C., McGurk, B., Ramirez, P., Richardson, M., Skiles, S. M., Seidel, F. C., & Winstral, A. (2016). The Airborne Snow Observatory: Fusion of scanning lidar, imaging spectrometer, and physically-based modeling for mapping snow water equivalent and snow albedo. Remote Sensing of Environment, 184, 139–152. https://doi.org/10.1016/j.rse.2016.06.018

Peitzsch, E., Fagre, D., Hendrikx, J., & Birkeland, K. (2018). DETECTING SNOW DEPTH CHANGE IN AVALANCHE PATH STARTING ZONES USING UNINHABITED AERIAL SYSTEMS AND STRUCTURE FROM MOTION PHOTOGRAMMETRY. Proceedings, International Snow Science Workshop 2018, Innsbruck, Austria, 5.

Prokop, A., Schön, P., Singer, F., Pulfer, G., Naaim, M., Thibert, E., & Soruco, A. (2015). Merging terrestrial laser scanning technology with photogrammetric and total station data for the determination of avalanche modeling parameters. Cold Regions Science and Technology, 8.

R Core Team. (2019). R: A Language and Environment for Statistical Computing. R Foundation for Statistical Computing. https://www.R-project.org/

Redpath, T. A. N., Sirguey, P., & Cullen, N. J. (2018). Repeat mapping of snow depth across an alpine catchment with RPAS photogrammetry. The Cryosphere, 12(11), 3477–3497. https://doi.org/10.5194/tc-12-3477-2018

Reuter, B., Richter, B., & Schweizer, J. (2016). Snow instability patterns at the scale of a small basin. Journal of Geophysical Research: Earth Surface, 121(2), 257–282. https://doi.org/10.1002/2015JF003700

Saloranta, T. M. (2016). Operational snow mapping with simplified data assimilation using the seNorge snow model. Journal of Hydrology, 538, 314–325. https://doi.org/10.1016/j.jhydrol.2016.03.061

Schweizer, J., & Kronholm, K. (2007). Snow cover spatial variability at multiple scales: Characteristics of a layer of buried surface hoar. Cold Regions Science and Technology, 47(3), 207–223. https://doi.org/10.1016/j.coldregions.2006.09.002

Schweizer, J., Kronholm, K., Jamieson, J. B., & Birkeland, K. W. (2008). Review of spatial variability of snowpack properties and its importance for avalanche formation. Cold Regions Science and Technology, 51(2–3), 253–272. https://doi.org/10.1016/j.coldregions.2007.04.009

Schweizer, J., Reuter, B., van Herwijnen, A., Richter, B., & Gaume, J. (2016). Temporal evolution of crack propagation propensity in snow in relation to slab and weak layer properties. The Cryosphere, 10(6), 2637–2653. https://doi.org/10.5194/tc-10-2637-2016

Smith, M. W., Carrivick, J. L., & Quincey, D. J. (2016). Structure from motion photogrammetry in physical geography. Progress in Physical Geography: Earth and Environment, 40(2), 247–275. https://doi.org/10.1177/0309133315615805

Smyth, E. J., Raleigh, M. S., & Small, E. E. (2020). Improving SWE Estimation With Data Assimilation: The Influence of Snow Depth Observation Timing and Uncertainty. Water Resources Research, 56(5). https://doi.org/10.1029/2019WR026853

Sproles, E. A., Nolin, A. W., Rittger, K., & Painter, T. H. (2013). Climate change impacts on maritime mountain snowpack in the Oregon Cascades. Hydrology and Earth System Sciences, 17(7), 2581–2597. https://doi.org/10.5194/hess-17-2581-2013

Sproles, Eric A., Mullen, A., Hendrikx, J., Gatebe, C., & Taylor, S. (2020). Autonomous Aerial Vehicles (AAVs) as a Tool for Improving the Spatial Resolution of Snow Albedo Measurements in Mountainous Regions. Hydrology, 7(3), 41. https://doi.org/10.3390/hydrology7030041

Statham, G., Haegeli, P., Greene, E., Birkeland, K., Israelson, C., Tremper, B., Stethem, C., McMahon, B., White, B., & Kelly, J. (2018). A conceptual model of avalanche hazard. Natural Hazards, 90(2), 663–691. https://doi.org/10.1007/s11069-017-3070-5

Takasu, T. (2009). RTKLIB: Open Source Program Package for RTK-GPS. FOSS4G Tokyo, Japan. http://gpspp.sakura.ne.jp/paper2005/foss4g_2009_rtklib.pdf

U.S. Geological Survey. (2017). USGS NED 1/3 arc-second n46w111 1 x 1 degree ArcGrid 2017 (published 20171130) [Map]. U.S. Geological Survey. https://www.usgs.gov/core-science-systems/ngp/3dep/data-tools

Van Peursem, K., Hendrikx, J., Birkeland, K., Miller, D., & Gibson, C. (2016). VALIDATION OF A COUPLED WEATHER AND SNOWPACK MODEL ACROSS WESTERN MONTANA. 9.

Vander Jagt, B., Lucieer, A., Wallace, L., Turner, D., & Durand, M. (2015). Snow Depth Retrieval with UAS Using Photogrammetric Techniques. Geosciences, 5(3), 264–285. https://doi.org/10.3390/geosciences5030264

Water Supply Forecasting Unit. (1984). Snow Survey Sampling Guide. In Soil Conservation Service, Agriculture Handbook Number 169. U.S. Department of Agriculture. https://www.wcc.nrcs.usda.gov/factpub/ah169/SnowSurveySamplingGuideHandout.pdf

Watts, A. C., Ambrosia, V. G., & Hinkley, E. A. (2012). Unmanned Aircraft Systems in Remote Sensing and Scientific Research: Classification and Considerations of Use. Remote Sensing, 4(6), 1671–1692. https://doi.org/10.3390/rs4061671

Wehr, A., & Lohr, U. (1999). Airborne laser scanning—An introduction and overview. ISPRS Journal of Photogrammetry and Remote Sensing, 54(2–3), 68–82. https://doi.org/10.1016/S0924-2716(99)00011-8

Westoby, M. J., Brasington, J., Glasser, N. F., Hambrey, M. J., & Reynolds, J. M. (2012). 'Structure-from-Motion' photogrammetry: A low-cost, effective tool for geoscience applications. Geomorphology, 179, 300–314. https://doi.org/10.1016/j.geomorph.2012.08.021

Wirz, V., Schirmer, M., Gruber, S., & Lehning, M. (2011). Spatio-temporal measurements and analysis of snow depth in a rock face. The Cryosphere, 5(4), 893–905. https://doi.org/10.5194/tc-5-893-2011

APPENDICES

APPENDIX A

GLOSSARY

Glossary 1. Parameters in Agisoft Metashape.

DEM Quality also operates similarly to *Dense Cloud Quality* and *Mesh Depth Map Quality* and determines the amount of image downscaling to be processed in DEM creation. Source refers to the source data for DEM interpolation and creation.

Dense Cloud Quality determines whether photos are downsampled before building the dense cloud and categorically relates to progressive downsizing of available pixels by a factor of 4.

Depth Filtering progressively filters out small outliers to clarify broad scenes as the setting increases (mild, moderate, and aggressive).

Estimated Image Quality is calculated by Agisoft Metashape and results in a unitless value based on the sharpness of focus within each image.

Face Count selects the ratio of polygons to dense cloud points with high, medium and low representing 1/5, 1/15, and 1/45, respectively.

Mesh - Depth Map Quality operates similarly to *Dense Cloud Quality* by using full resolution or progressively downsampled images for mesh creation.

Photo Alignment - Key Point Limit is the maximum number of points in every image to be utilized during initial alignment.

Photo Alignment - Tie Point Limit is the maximum number of matching points in every image utilized during initial alignment.

Projection Accuracy is a unitless value which allows for the filtering of points with pixel matching errors.

Reconstruction Uncertainty is a unitless value which allows for the filtering of points with poor geometry that lead to noise in the point cloud.

Reproduction Error is a unitless value which allows for the filtering of points with poor location accuracy and false point matches.

APPENDIX B

TABLES

Appendix Table 1. Description of sampling day flight conditions and collection parameters

Acquisition Date	Sky Condition	Temperature (°C)	Mean Flight Height (m a.g.l.)	GSD (cm/pix)	Images Collected	Coverage Area (km²)
20200107	OVC	0.5	45.8	1.18	768	0.093
20200110	FEW	-8.9	70.9	1.85	350	0.141
20200115	CLR	-15.0	64.7	1.72	598	0.183
20200204	CLR	-15.0	71.2	1.81	513	0.218
20200213	SCT	-1.5	67.2	1.58	519	0.205
20200221	CLR	-1.2	67.4	1.75	572	0.175
20200227	CLR	-4.2	67	1.77	571	0.187
20200306	SCT	2.0	61.9	1.63	571	0.195
20200310	FEW	-6.4	67	1.75	571	1.91
20200317	CLR	2.4	66.9	1.75	571	0.192
20200514	BKN	4.6	62.3	1.59	562	0.19
20200525	CLR	8.0	62.4	1.67	562	0.203
20200709	BKN	16.1	67.4	1.76	563	0.179

Appendix Table 2. Summary of snow depths (SD) measured for sampling days.

Sampling day	Brackett Meadow AWS measured SD (cm)	Mean Measured SD (cm)	Measured SD Range (cm)	Modeled mean SD at Measured Locations (cm)	Modeled SD Range (cm)	Mean Difference Between Measured SD and Modeled SD	RMSE of Difference Between Measured SD and Modeled SD	Standard Deviation of Difference Between Measured SD and Modeled SD
20200107	96.3	116.2	9	123.3	31.2	7.1	14.7	15.8
20200110	111.2	122.2	13	236.4	9.5	114.2	114.3	4.9
20200115	122.3	141.4	10.6	180	28.4	38.6	41.1	17.3
20200204	151.0	173.1	11.4	274.3	59.4	101.2	103.5	26.5
20200213	221.9	259.1	111.4	227.5	62.8	-31.6	85.7	97.6

20200221	211.0	212.4	120	239.4	425.1	27	109.5	110.5
20200227	210.5	225.9	28.8	203.4	40.8	-22.5	33.6	28.8
20200306	190.3	194.7	79	179.3	150.5	-15.5	36.6	34.5
20200310	206.6	211.7	17.2	169.5	163.1	-42.1	73.5	69.5
20200317	200.7	211.4	19.8	235.4	57	24	30.8	22.2
20200514	157.4	174.8	65.2	191.9	342.4	30.6	80.6	77.4
20200525	118.9	136.7	14.4	151.4	17.3	14.7	16.6	8.7

Appendix Table 3. Mean CV and standard deviation of CV for seasonal snow depth and snow depth change.

Window Size	**Hourglass Seasonal Snow Depth mean CV % (standard deviation of CV %)**	**Brackett Meadow Seasonal Snow Depth mean CV % (standard deviation of CV %)**	**Hourglass Snow Depth Change mean CV % (standard deviation of CV %)**	**Brackett Meadow Snow Depth Change mean CV % (standard deviation of CV %)**
10 cm	60 (10)	43 (5)	65 (20)	48 (15)
25 cm	60 (15)	56 (8)	68 (27)	62 (19)
50 cm	63 (22)	53 (13)	75 (35)	63 (25)
100 cm	67 (34)	57 (25)	84 (48)	69 (35)

APPENDIX C

FIGURES

Appendix Figure 1. Natural avalanche crown profile.

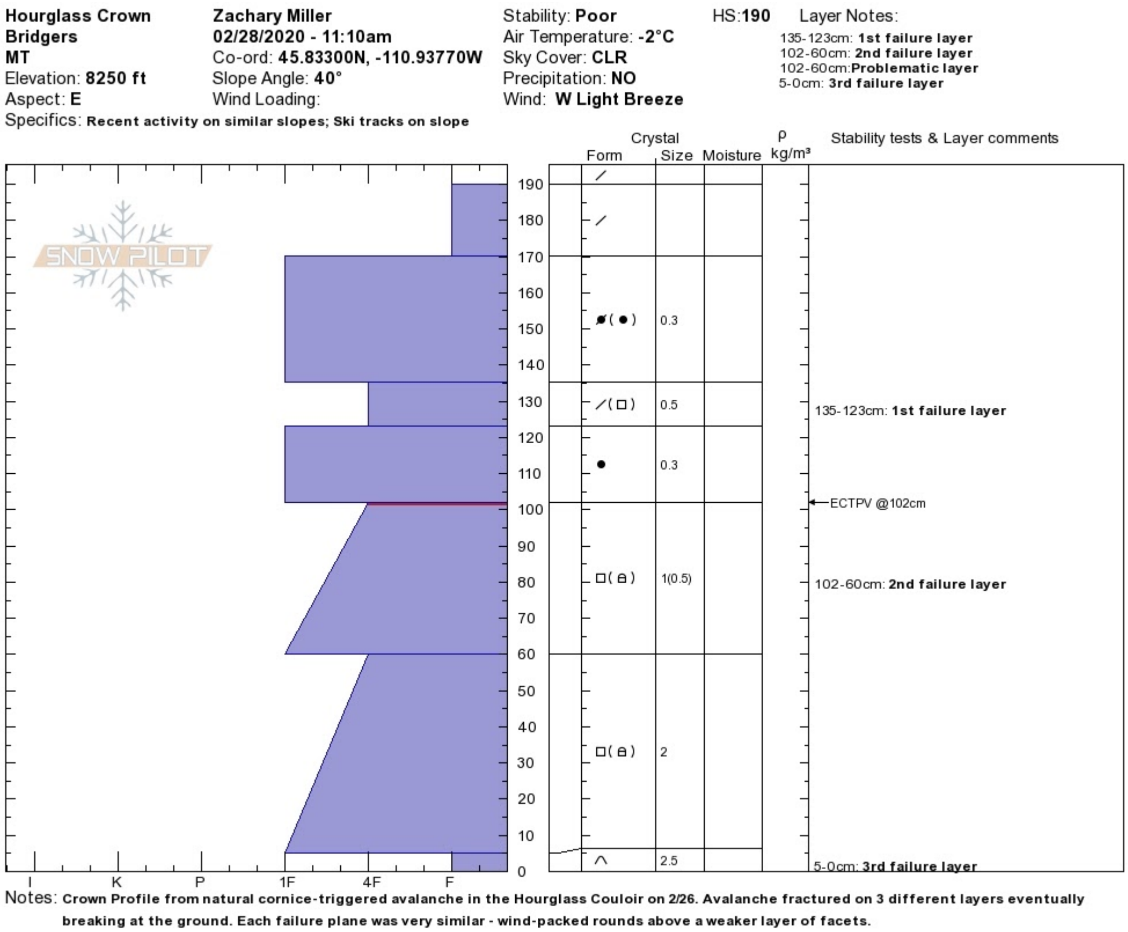

Appendix Figure 2. Natural avalanche overview image.

Appendix Figure 3. Natural avalanche start zone image.